EUROPEAN ORGANIZATION FOR NUCLEAR RESEARCH

CERN/EP 81-51
2 June 1981

INCLUSIVE Λ AND $\bar{\Lambda}$ PRODUCTION IN K^+p INTERACTIONS AT 70 GeV/c

Brussels-CERN-Genova-Mons-Nijmegen-Serpukhov Collaboration

M. Barth(*), C. De Clercq(*), E.A. De Wolf(**), J.J. Dumont(*),
D.P. Johnson(*), J. Lemonne and P. Peeters
Inter-University Institute for High Energies (ULB-VUB), Brussels, Belgium

H. Drevermann, Y. Goldschmidt-Clermont, G. Harigel, C. Milstene(***),
J.P. Porte, R.T. Ross, M. Spyropoulou-Stassinaki, S. Squarcia(+),
P. Theocharopoulos and G. Vassiliadis(++)
CERN, European Organization for Nuclear Research, Geneva, Switzerland

C. Caso, R. Contri, F. Fontanelli, R. Monge and U. Trevisan
Sezione INFN and Istituto di Scienze Fisiche, Genova, Italy

J.F. Baland, J. Beaufays, J. Hanton and F. Grard
Faculté des Sciences, Université de l'Etat, Mons, Belgium

P.A. van der Poel, L. Gatignon, W. Kittel, W.J. Metzger, D.J. Schotanus,
A. Stergiou and R.T. Van de Walle
University of Nijmegen, Nijmegen, Netherlands

Y. Belokopitov, P. Chliapnikov, A. Fenyuk, L. Gerdyukov, I. Gritsaenko,
G. Khromova, V. Kubic, S. Lugovsky, V. Nikolaenko, Y. Petrovykh. V. Ronjin,
A. Vorobjev and V. Yarba
Institute for High Energy Physics, Serpukhov, USSR(++)

Submitted to Zeitschrift für Physik C

(*) Chercheur IISN/Navorser IIKW.

(**) Bevoegdverklaard Navorser NFWO Belgium. Also at Universitaire Instelling Antwerpen, Belgium.

(***) Visitor from Tel-Aviv University, Tel-Aviv, Israel.

(+) On leave of absence from Genova University, Genova, Italy.

(++) Visitor from University of Athens, Greece.

(+++) Participating under the terms of the 1967 agreement between CERN and the USSR State Committee for the Utilization of Atomic energy.

0024P/PT/ed

ABSTRACT

Inclusive and semi-inclusive production of Λ and $\bar{\Lambda}$ in K^+p interactions is studied at an incident momentum of 70 GeV/c. Cross sections and single particle distributions are presented and compared with data at lower energies. Scaling is observed between 32 and 70 GeV/c in the Feynman x variable in the target and the beam fragmentation regions for Λ and $\bar{\Lambda}$ inclusive production respectively. An increase of $\Lambda(\bar{\Lambda})$ production is observed in the beam (target) fragmentation regions, whereas the data at 70 and 32 GeV/c are reasonably close in the central region. The dependence of the $\Lambda(\bar{\Lambda})$ polarization as a function of x is measured and found to be in general agreement with the results at 32 GeV/c. The $(\Lambda\bar{\Lambda})$ pair production cross section increases significantly from 32 to 70 GeV/c. The Λ and $\bar{\Lambda}$ production associated with an identified proton is also studied.

1. INTRODUCTION

In this paper we present results from an analysis of the inclusive Λ and $\bar{\Lambda}$ production in K^+p interactions at an incident momentum of 70 GeV/c, using data from an exposure of the Big European Bubble Chamber (BEBC).

In similar studies at lower beam momenta, 8.2, 12.7, 16 and 32 GeV/c [1-3], scaling is not observed in the Feynman x variable although early scaling conditions [4] are satisfied in the beam and the target fragmentation regions for Λ and in the beam fragmentation region for $\bar{\Lambda}$. However, in the 32 GeV/c data, [3], dominance of target and beam fragmentation processes is demonstrated for Λ and $\bar{\Lambda}$ production respectively. Thus, the extension of the study of $\Lambda(\bar{\Lambda})$ inclusive production to 70 GeV/c is of interest.

The reactions studied here are

$$K^+p \to \Lambda + X^{++} \tag{1}$$

$$K^+p \to \bar{\Lambda} + X^{++} \tag{2}$$

and the semi-inclusive production processes

$$K^+p \to \Lambda\bar{\Lambda} + X^{++} \tag{3}$$

$$K^+p \to \Lambda p_{slow} + X^{+} \tag{4}$$

$$K^+p \to \bar{\Lambda} p_{slow} + X^{+} \quad . \tag{5}$$

We also estimate the cross sections for the reactions

$$K^+p \to \Sigma^{*+}_{1385} + X^{+} \tag{6}$$

$$K^+p \to \Sigma^{*-}_{1385} + X^{+++} \quad . \tag{7}$$

In sect. 2, the experimental procedure, the data sample used and cross section results are presented. The differential cross sections for reactions (1) and (2) are presented in sect. 3, and wherever possible comparisons with the results in lower energies are made. In sect. 4, reactions (3), (4) and (5) are studied and finally the conclusions are summarized in sect. 5.

2. EXPERIMENTAL PROCEDURE AND CROSS SECTIONS

The data were obtained from an exposure of BEBC, filled with hydrogen, to an r.f. separated K^+ beam of 70 GeV/c nominal momentum. Details of the experimental set-up and the total, elastic and topological cross sections for K^+p interactions at 70 GeV/c are given in a previous publication [5].

The present analysis is based on a sample of $\sim$ 51 000 events corresponding to a sensitivity of $\sim$ 2.8 events per microbarn. After double scanning, measurement and remeasurement, all events were processed through the Hydra geometry program. A modified version of the Hydra kinematics optimized for V^0/γ fitting, [6], was then used to fit the usual hypotheses for K^n, Λ, $\bar{\Lambda}$ decay and e^+e^- pair production at each V^0/γ vertex(*).

Only 3C fit unambiguous $\Lambda(\bar{\Lambda})$ events associated to an even topology primary vertex were considered. The obtained samples of 1152 Λ and 518 $\bar{\Lambda}$ events were appropriately weighted for the following momentum dependent losses: (a) decays outside the fiducial volume, (b) decays very close to the production vertex, (c) secondary interactions, (d) K^n/Λ and $K^n/\bar{\Lambda}$ ambiguities. In the latter case the "Podolansky-Armenteros" method was applied, [7], as described in ref. [8].

Finally, correction factors for scanning efficiency (97%) and data processing efficiency (94%) were used which lead to an overall systematic error of 2%. No attempt has been made in the present analysis to distinguish between directly produced Λ's ($\bar{\Lambda}$'s) and those resulting from Σ^0's ($\bar{\Sigma}^0$'s) decays.

Using the aforementioned experimental procedure and the topological cross sections of ref. [5] we obtain for the total $\Lambda(\bar{\Lambda})$ cross sections the values: $\sigma_\Lambda = 1.09 \pm 0.05$ mb and $\sigma_{\bar{\Lambda}} = 0.65 \pm 0.04$ mb. These values are given in table 1 together with the topological cross sections for reactions (1) and (2).

(*) A paper dealing with the neutral kaon production is forthcoming.

In fig. 1 we compare the total $\Lambda(\bar{\Lambda})$ inclusive cross sections of this experiment with those at lower energies. The cross sections increase approximately as $\ell n s$. In fig. 2 the topological cross sections for reactions (1) and (2), at lab momenta from 8 to 70 GeV/c, are presented. The general feature in this figure is the increase of the higher multiplicity cross sections with increasing energy. More specifically in fig. 2(a) and 2(b) the 2-prong cross section decreases between 32 and 70 GeV/c, whereas the 4-prong cross section is almost constant and for 6-prong and above the cross sections increase with increasing energy.

In table 1 the cross sections for reactions (3)-(7) are also presented. The cross sections for reactions (4) and (5) were calculated from the number of $\Lambda(\bar{\Lambda})$ events with an identified proton ($p_{lab} < 1.2$ GeV/c) [9].

The estimation of $\Sigma^{*\pm}_{1385}$ cross sections was made by fitting to the $d\sigma/dM_{\Lambda\pi^\pm}$ experimental distributions, fig. 3, the following expression

$$d\sigma/dM = (1 + a_1 \cdot BW) \cdot BG \tag{8}$$

where,

$$BG = a_2(M - M_{th})^{a_3} \cdot \exp[-a_4(M - M_{th}) - a_5(M - M_{th})^2] \tag{9}$$

and BW is the relativistic Breit-Wigner function. Comparison of the cross sections for $\Sigma^{*\pm}_{1385}$ with data obtained at 32 GeV/c, [10], suggests that the fraction of Λ's coming from $\Sigma^{*\pm}_{1385}$ resonances is about the same at both energies, ($\sim$ 25%), for identical parametrizations of the background.

3. SINGLE PARTICLE INCLUSIVE DISTRIBUTIONS

3.1 General features

The Chew-Low plots for reactions (1) and (2) are shown in fig. 4. In both reactions the data accumulate near the boundaries of the plots, as expected, mainly in the high mass regions and are consistent with a dominant production of $\Lambda(\bar{\Lambda})$ in the target (beam) fragmentation region. Figs 5 and 6, show the projections of the Chew-Low plots together with data at lower energies. The M_x^2/s distributions at 70 and 32 GeV/c are seen to be compatible for $M_x^2/s \leq 0.7$ whereas the four momentum transfer distributions, fig. 6, start to differ for $|t| \geq 2(\text{GeV/c})^2$, for both Λ and $\bar{\Lambda}$ production.

3.2 Longitudinal momentum distributions

The invariant Feynman x distributions for reactions (1) and (2),

$$f(x) = \int_{p^*_{max}} \frac{E^*}{} \frac{d^2\sigma}{dx \cdot dp_T^2} dp_T^2 \qquad (10)$$

are shown in fig. 7 and given also in table 2(*). These distributions clearly show that Λ's are produced preferentially in the target fragmentation region, whereas the $\bar{\Lambda}$'s are produced mainly forwards, i.e. in the beam fragmentation region. This effect is quantified in the forward-backward asymmetry values and average x values given in table 3.

Fits of the expression $A(1 - |x|)^n$ to the experimental invariant x distributions for reactions (1) and (2) yield the values of n given in table 4. Within the limited statistics the values obtained are in general agreement with the predictions of the quark counting rules based on a gluon exchange hadronic interaction mechanism with point-like sea-quark pair production [11], as also found for lower energy data [12].

It is interesting to compare the f(x) distributions at 70 GeV/c with the corresponding distributions from lower energies, [1,3], as shown in fig. 7. In both Λ and $\bar{\Lambda}$ inclusive production, these distributions are near to scaling between 70 and 32 GeV/c over the full x region. Closer inspection reveals that for reaction (1) scaling is present for the region $x < -0.4$ and for reaction (2) for the region $x > 0.2$. Outside these regions the distributions from 70 GeV/c tend to lie systematically above the 32 GeV/c data. This is particularly evident for the backward $\bar{\Lambda}$ production.

The regions where $\Lambda/\bar{\Lambda}$ production is higher at 70 GeV/c than at 32 GeV/c are more clearly identified in the rapidity distributions, fig. 8. A shoulder appears at $y^* \sim 0.8$ for Λ and at $y^* \sim -0.8$ for $\bar{\Lambda}$, suggesting a rising contribution of the beam (target) fragmentation component in the $\Lambda(\bar{\Lambda})$ production. The rise of the Λ production from the kaon fragmentation component (already indicated at lower energies) could be attributed to the contribution of the u-valence quark recombination process (as, for example,

---

(*) We have omitted the constant $1/\pi$ factor for direct comparison with other data.

in the $\pi^+ p \to \Lambda$ fragmentation processes at 32 GeV/c [13]). However, the $\bar{\Lambda}$ target fragmentation component (not seen at lower energies) cannot be explained by such a process. We note that the observation of the rise of the beam (target) fragmentation processes could be easily missed if the central $\Lambda(\bar{\Lambda})$ production processes were also increasing. In figs 7 and 8 the data at 70 and 32 GeV/c are reasonably close in the central region. Similar conclusions are suggested by the comparison of the Λ inclusive x and y^* distributions in $K^- p$ interactions at 110 GeV/c with lower energy data, [14], where the decrease in the hypercharge annihilation channel with increasing energy is not compensated by an increase of the central Λ production.

3.3 Transverse momentum distributions

The differential cross sections as functions of p_T^2 for reactions (1) and (2) are shown in figs 9(a) and 9(b) and the average values of p_T and p_T^2 are given in table 3. The corresponding data from lower energies, [1,3], are also presented in these figures.

All distributions exhibit an approximate exponential behaviour. The values of the slope parameter b, resulting from a least squares fit to the expression

$$\frac{d\sigma}{dp_T^2} = A \cdot \exp(-bp_T^2) \qquad (11)$$

are given in table 5. From this table it is clear that the slope decreases with increasing energy. Further, the slopes for reactions (1) and (2) are very similar at least above 16 GeV/c and for the 70 GeV/c data the values of $\langle p_T \rangle$ and $\langle p_T^2 \rangle$ (table 3) are the same for the two reactions.

The variation of the average transverse momentum, $\langle p_T \rangle$, as a function of x is presented in figs 10(a) and 10(b), for reactions (1) and (2) respectively, and compared with the 32 GeV/c data. For both energies the distributions are consistent for reaction (1) for $x < 0.4$ and for reaction (2) for $x > -0.2$. The small but systematic rise of $\langle p_T \rangle$ for $x > 0.4$ for reaction (1) may be a reflection of the rise in the beam fragmentation processes mentioned in sect. 3.2.

3.4 Polarization

The polarization of the $\Lambda(\bar{\Lambda})$ was determined from the $\Lambda \to p\pi^-$ ($\bar{\Lambda} \to \bar{p}\pi^+$) decay, using the formula [15]

$$\alpha P \pm \Delta(\alpha P) = \frac{\langle \cos\theta_N \rangle}{\langle \cos^2\theta_N \rangle} \pm \frac{1}{\sqrt{N}} \frac{[\langle \cos^2\theta_N (1 - \alpha P \cos\theta_N)^2 \rangle]^{1/2}}{\langle \cos^2\theta_N \rangle} \qquad (12)$$

where,

θ_N: is the angle between the normal to the production plane and the direction of the decay proton (antiproton) in the $\Lambda(\bar{\Lambda})$ rest frame.

N: is the total number of events.

α: is the weak decay asymmetry parameter with value: $\alpha = 0.642 \pm 0.013$ for Λ's and $\alpha = -0.642 \pm 0.013$ for $\bar{\Lambda}$'s.

The normal to the production plane is defined as:

$$\hat{n} = (\bar{p}_{\Lambda(\bar{\Lambda})} \times \bar{p}_{p(K)}) / |\bar{p}_{\Lambda(\bar{\Lambda})} \times \bar{p}_{p(K)}| \quad . \qquad (13)$$

The average value of the polarization was found to be $P(\Lambda) = 0.10 \pm 0.05$ and $P(\bar{\Lambda}) = -0.18 \pm 0.07$ for Λ's and $\bar{\Lambda}$'s respectively. The variation of P as a function of x is shown in figs 11(a) and 11(b). The data at 13 and 32 GeV/c, [15], are also presented for comparison. The distribution for reaction (1), fig. 11(a), is consistent with the lower energy data and there is no evidence for polarization over the full x region. On the other hand, our data for reaction (2), fig. 11(b), exhibit a behaviour similar to that at 32 GeV/c with a negative polarization in the high x forward region.

4. $(\Lambda\bar{\Lambda})$, (Λp_{slow}) AND $(\bar{\Lambda} p_{slow})$ PRODUCTION

In this section a study of reactions (3), (4) and (5) is presented. The sample used and the corresponding total and topological cross sections for these reactions are discussed in sect. 2 and presented in table 1.

The scatter plots of the individual x variables for the particles of each pair are presented in figs 12(a), 12(b) and 12(c) for reactions (3), (4) and (5) respectively.

In fig. 12(a) it is observed that the Λ's and $\bar{\Lambda}$'s are produced mainly at small x values. This can be interpreted as an indication that the $(\Lambda\bar{\Lambda})$ pairs are produced by a multiperipheral mechanism. Alternatively, contributions from fragmentation processes of the type $K^+ \to (\bar{\Xi}\Lambda)X$ would tend to give the observed Λ and $\bar{\Lambda}$ at small x values. The present level of statistics is insufficient to distinguish between these and other similar processes.

The distribution of the points in figs 12(b) and 12(c) as a function of x_p is directly influenced by the slow proton selection.

From fig. 12(c) it is seen that the general features of inclusive $\bar{\Lambda}$ production are independent of the presence of the slow proton as expected from the dominance of the K^+ fragmentation processes for $\bar{\Lambda}$ production. Indeed, as $\bar{\Lambda}$ carries the massive $\bar{s}$ quark of the projectile it is expected to be produced in the positive x region.

The Λ production in the process of reaction (4) appears to be less central than that observed in reaction (3) (fig. 12(b) and table 3). Although this could be due to a preferential selection of K^+ fragmentation processes, such as $K^+p \to \Lambda\bar{X} + X$, it could also be due to a kinematical bias induced by the trigger on slow protons with x near -1. The same remark applies when comparing the characteristics of inclusive Λ's produced with a slow proton to the results of reaction (1).

Finally, comparison of our data with the data at 32 GeV/c, [3], shows an increase of the cross sections for reactions (3), (4) and (5) (for reaction (5) comparatively smaller) but a similar behaviour for all reactions in the x scatter plots at 32 and 70 GeV/c.

5. CONCLUSIONS

The conclusions of the study of Λ and $\bar{\Lambda}$ production in K^+p interactions at 70 GeV/c are summarized as follows:

(a) The total cross sections at 70 GeV/c are: $\sigma_\Lambda = 1.09 \pm 0.05$ mb and $\sigma_{\bar{\Lambda}} = 0.65 \pm 0.04$ mb increasing approximately as &ns. Moreover, the cross sections for multiplicities above four are increasing rapidly above 32 GeV/c.

(b) Λ's are produced preferentially in the target fragmentation region and $\bar{\Lambda}$'s are mainly produced in the beam fragmentation region. In these regions the reactions (1) and (2) are consistent with scaling between 32 GeV/c and 70 GeV/c.

(c) The slopes of the $d\sigma/dp_T^2$ distributions for Λ's and $\bar{\Lambda}$'s are essentially the same, but these slopes for both reactions are decreasing with increasing energy.

(d) Polarization for Λ is consistent with zero over the complete x range, whereas the $\bar{\Lambda}$ data show negative polarization values in the forward direction, in agreement with the 32 GeV/c data.

(e) The inclusive $(\bar{\Lambda}p_{slow})$ and especially the $(\Lambda\bar{\Lambda})$ and (Λp_{slow}) cross sections increase with increasing energy.

REFERENCES

[1] P.V. Chliapnikov et al., Nucl. Phys. B112 (1976) 1.

[2] W. Barletta et al., Nucl. Phys. B51 (1973) 499.

[3] P.V. Chliapnikov et al., Nucl. Phys. B131 (1977) 93.

[4] Chan Hong-Mo et al., Phys. Rev. Lett. 26 (1971) 672.

[5] M. Barth et al., Z. Physik C, Part. and Fields, 2 (1979) 285.

[6] CERN HYDRA Applications Library.

[7] J. Podolanski and R. Armenteros, Phil. Mag. 45 (1954) 13.

[8] C. Cochet et al., Nucl. Phys. B124 (1977) 61.

[9] M. Barth et al., Z. Physik C, Part. and Fields, 7 (1981) 89.

[10] I.V. Ajinenko et al., IHEP 80-129 (1980).

[11] J.F. Gunion, Phys. Lett. 88B (1979) 150.

[12] D. Denegri et al., Phys. Lett. 98B (1981) 127.

[13] I.V. Ajinenko et al., Nucl. Phys. B165 (1980) 1.

[14] P.R.S. Wright et al., CERN/EP 81-2 (1981), Submitted to Nucl. Phys. B.

[15] M.L. Faccini-Turluer et al., Z. Physik C, Part. and Fields, 1 (1979) 16.

TABLE CAPTIONS

TABLE 1 Total and topological cross sections for Λ and $\bar{\Lambda}$ production in K^+p interactions at 70 GeV/c.

TABLE 2 The dependence of the structure function on the Feynman x variable for reactions (1) and (2) at 70 GeV/c.

TABLE 3 Asymmetry A and the average values of x, p_T and p_T^2 for reactions (1) to (5) at 70 GeV/c. [σ_F (σ_B) refers to the cross section for $x > 0$ ($x < 0$)].

TABLE 4 Values of n resulting from fits of the expression $A(1 - |x|)^n$ to the experimental data at 70 GeV/c.

TABLE 5 Values of the exponential slope parameter b of the p_T^2 distributions.

TABLE 1

Reaction	Topological cross section (μb)							Total mb
	2-prong	4-prong	6-prong	8-prong	10-prong	12-prong	14-prong	
$K^+p \to \Lambda + X^{++}$	105 ± 14	299 ± 26	303 ± 26	218 ± 21	112 ± 14	39 ± 7	12 ± 4	1.09 ± 0.05
$K^+p \to \bar{\Lambda} + X^{++}$	81 ± 15	178 ± 21	182 ± 20	134 ± 16	51 ± 9	22 ± 6	2 ± 2	0.65 ± 0.04
$K^+p \to \Lambda\bar{\Lambda} + X^{++}$		26 ± 10	35 ± 12	10 ± 6	11 ± 8	2 ± 2		0.08 ± 0.02
$K^+p \to \Lambda p_{s\ell} + X^+$	17 ± 6	36 ± 9	16 ± 5	14 ± 6	6 ± 3	1 ± 1		0.09 ± 0.01
$K^+p \to \bar{\Lambda} p_{s\ell} + X^+$	38 ± 10	57 ± 12	46 ± 10	30 ± 9	14 ± 7	3 ± 2		0.19 ± 0.02
$K^+p \to \Sigma^{*+}_{1385} + X^+$								0.20 ± 0.06
$K^+p \to \Sigma^{*-}_{1385} + X^{+++}$								0.07 ± 0.05

TABLE 2

	$f(x) = \int_{p^*_{max}}^{E^*} \frac{d^2\sigma}{dx \cdot dp_T^2} dp_T^2$	
x_F	Λ	$\bar{\Lambda}$
(-1.0) - (-0.9)	51 ± 26	
(-0.9) - (-0.8)	213 ± 44	
(-0.8) - (-.07)	269 ± 43	7 ± 5
(-0.7) - (-0.6)	341 ± 45	
(-0.6) - (-0.5)	422 ± 45	11 ± 5
(-0.5) - (-0.4)	503 ± 45	
(-0.4) - (-0.3)	527 ± 42	30 ± 10
(-0.3) - (-0.2)	413 ± 35	99 ± 17
(-0.2) - (-0.1)	342 ± 30	118 ± 17
(-0.1) - 0.0	333 ± 28	152 ± 19
0.0 - 0.1	233 ± 25	235 ± 25
0.1 - 0.2	201 ± 26	295 ± 33
0.2 - 0.3	168 ± 30	347 ± 42
0.3 - 0.4	98 ± 26	375 ± 53
0.4 - 0.5	59 ± 20	201 ± 33
0.5 - 0.6		
0.6 - 0.7	41 ± 18	79 ± 33
0.7 - 0.8		
0.8 - 0.9		
0.9 - 1.00		

TABLE 3

Reaction	$A = \frac{\sigma_F - \sigma_B}{\sigma_F + \sigma_B}$	$\langle x \rangle$	$\langle p_T \rangle$	$\langle p_T^2 \rangle$
$K^+p \to \Lambda + X^{++}$	$-.48 \pm .04$	$-.19 \pm .01$	$.51 \pm .01$	$.35 \pm .01$
$K^+p \to \bar{\Lambda} + X^{++}$	$.53 \pm .05$	$.16 \pm .01$	$.51 \pm .01$	$.35 \pm .02$
Λ_+ from $K^+p \to \Lambda\bar{\Lambda} + X^{++}$	$-.04 \pm .02$	$-.03 \pm .05$	$.64 \pm .07$	$.52 \pm .10$
$\bar{\Lambda}_+$ from $K^+p \to \Lambda\bar{\Lambda} + X^{++}$	$.25 \pm .11$	$.07 \pm .03$	$.50 \pm .05$	$.32 \pm .06$
Λ_+ from $K^+p \to \Lambda p_{s\ell} + X^+$	$.28 \pm .09$	$.11 \pm .05$	$.44 \pm .04$	$.28 \pm .04$
$\bar{\Lambda}_+$ from $K^+p \to \Lambda p_{s\ell} + X^+$	$.65 \pm .17$	$.22 \pm .02$	$.51 \pm .03$	$.37 \pm .05$

TABLE 4

	x region	n	χ^2/ND
$K^+ \to \Lambda$	0.8 - 0.2	1.66 ± 0.76	2.6/2
$K^+ \to \bar{\Lambda}$	0.8 - 0.3	2.14 ± 0.57	0.15/1
$p \overset{K^+}{\to} \Lambda$	(-1.0) - (-0.3)	0.77 ± 0.09	2.1/5
$p \overset{K^+}{\to} \bar{\Lambda}$	(-0.8) - (-0.2)	6.00 ± 1.60	3.0/2

TABLE 5

Beam momentum (GeV/c)	$K^+p \to \Lambda + X^{++}$		$K^+p \to \bar{\Lambda} + X^{++}$	
	p_T^2 interval $(GeV/c)^2$	b $(GeV/c)^{-2}$	p_T^2 interval $(GeV/c)^2$	b $(GeV/c)^{-2}$
8.2	0.0 - 1.92	4.16 ± 0.17	0.0 - 1.28	5.57 ± 0.40
16.0	0.0 - 1.92	3.46 ± 0.11	0.0 - 1.76	3.96 ± 0.20
32.0	0.0 - 1.90	3.21 ± 0.09	0.0 - 2.00	3.11 ± 0.14
70.0	0.0 - 2.25	3.01 ± 0.12	0.0 - 1.95	3.00 ± 0.18

FIGURE CAPTIONS

Fig. 1 Inclusive Λ, $\bar{\Lambda}$ cross sections as a function of the c.m. energy squared and of the incident K^+ momentum.

Fig. 2 (a)-(b) Topological cross sections for Λ and $\bar{\Lambda}$ production versus the incident momentum. The lines are drawn to guide the eye.

Fig. 3 (a)-(b) Effective mass distribution of the $(\Lambda\pi^{\pm})$ system. The curves are the results of a fit using the $\Sigma^{*\pm}_{1385}$ resonance and the background (relation (8)).

Fig. 4 (a)-(b) Chew-Low plots for reactions (1) and (2) at 70 GeV/c. The lines correspond to several constant values of $x = P^*_L/P^*_{max}$.

Fig. 5 (a)-(b) M^2_x/s distributions for reactions (1) and (2) at 70 and 32 GeV/c.

Fig. 6 The differential cross sections $d\sigma/dt$ for reactions (1) and (2) at 8.2, 16, 32 and 70 GeV/c.

Fig. 7 (a)-(b) The dependence of the structure function, integrated over P^2_T, on the Feynman x variable at 8.2, 16, 32 and 70 GeV/c incident momenta for reactions (1) and (2). The curves are the $(1 - |x|)^n$ fits described in the text.

Fig. 8 (a)-(b) The differential cross sections $d\sigma/dy^*$, at 8.2, 16, 32 and 70 GeV/c for reactions (1) and (2) respectively.

Fig. 9 (a)-(b) The differential cross sections $d\sigma/dp^2_T$ for 8.2, 16, 32 and 70 GeV/c data for reactions (1) and (2) respectively. The lines are the results of the fits of expresssion (11) to the data.

Fig. 10 (a)-(b) The dependence of the $\langle p_T \rangle$ on the $x = P^*_L/P^*_{inc}$ at 32 and 70 GeV/c incident momenta for reactions (1) and (2) respectively.

FIGURE CAPTIONS (Cont'd)

Fig. 11 (a)-(b) Polarization of $\Lambda(\bar{\Lambda})$'s as a function of x, for reactions (1) and (2) respectively at 13, 32 and 70 GeV/c.

Fig. 12 (a)-(c) x_F scatter plots for $(\Lambda\bar{\Lambda})$, (Λp_{slow}) and $(\bar{\Lambda} p_{slow})$ respectively, at 70 GeV/c.

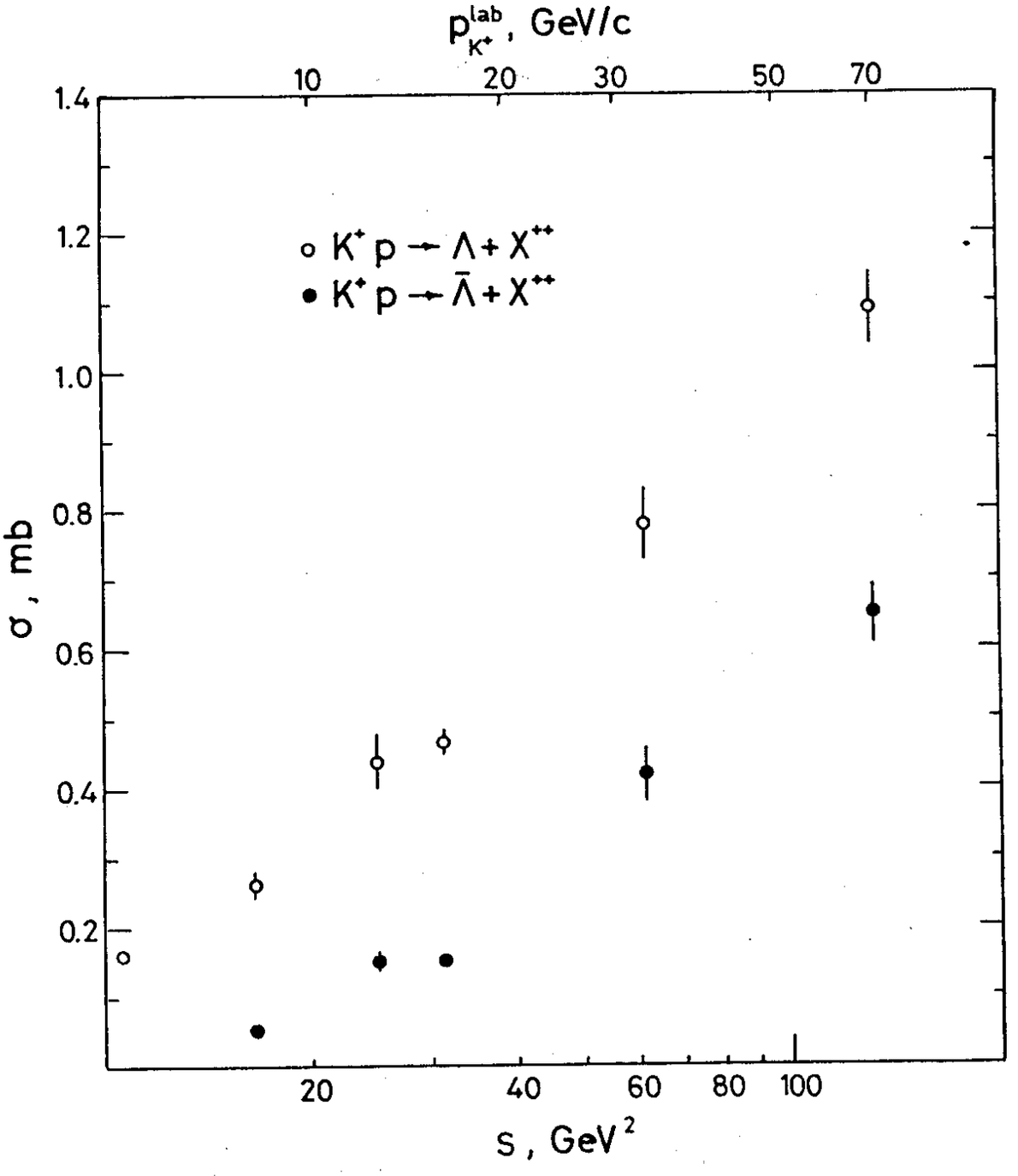
$p^{lab}_{K^+}$, GeV/c
10
20
30
50
70
1.4
1.2
1.0
0.8
0.6
0.4
0.2
σ, mb
$K^+ p \to \Lambda + X^{++}$
$K^+ p \to \bar{\Lambda} + X^{++}$
20
40
60
80
100
S, GeV^2

Fig. 1

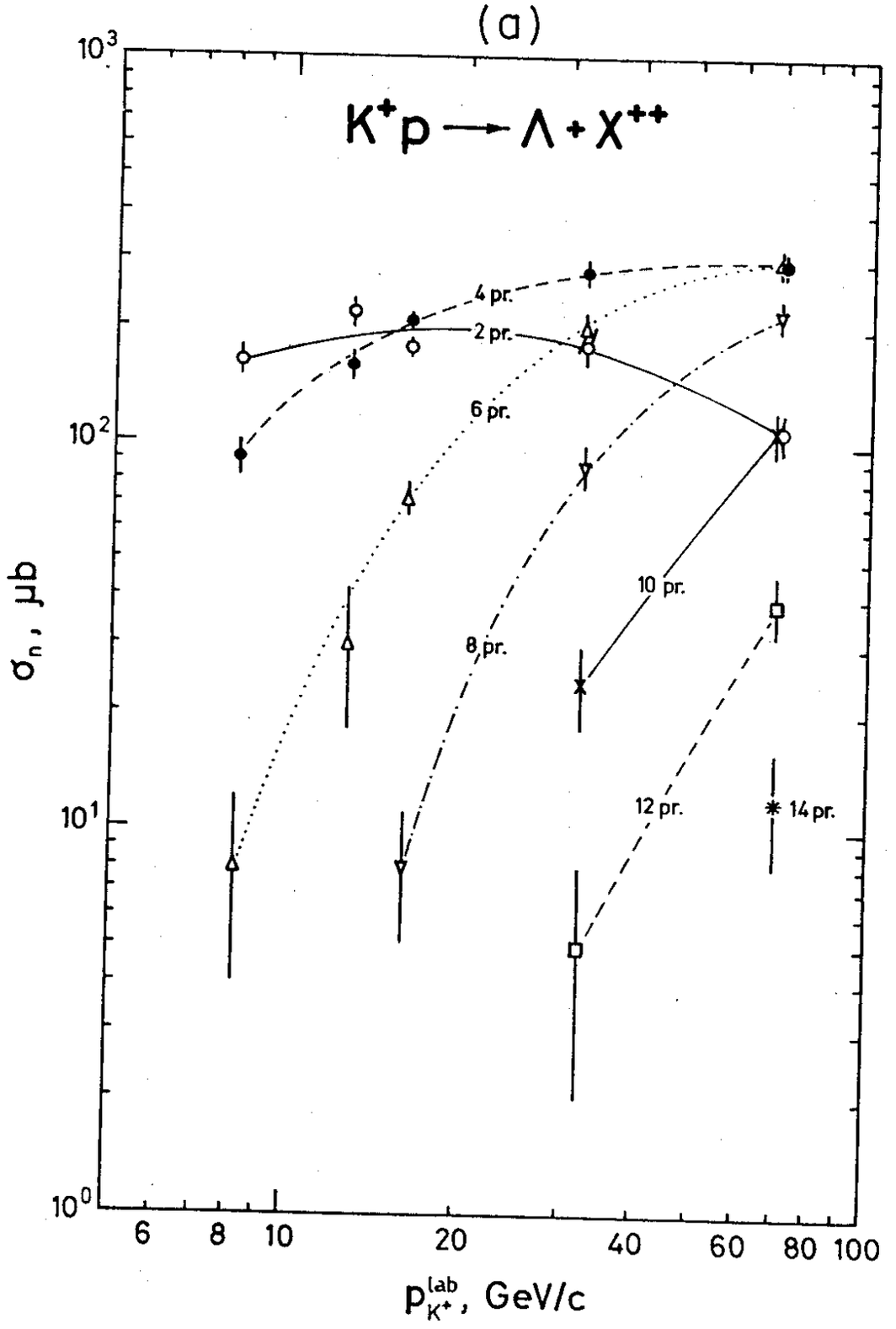
(a)
$K^+p \rightarrow \Lambda + X^{++}$
10^3
10^2
10^1
10^0
σ_n, μb
4 pr.
2 pr.
6 pr.
8 pr.
10 pr.
12 pr.
14 pr.
6
8
10
20
40
60
80
100
$p^{lab}_{K^+}$, GeV/c

Fig. 2(a)

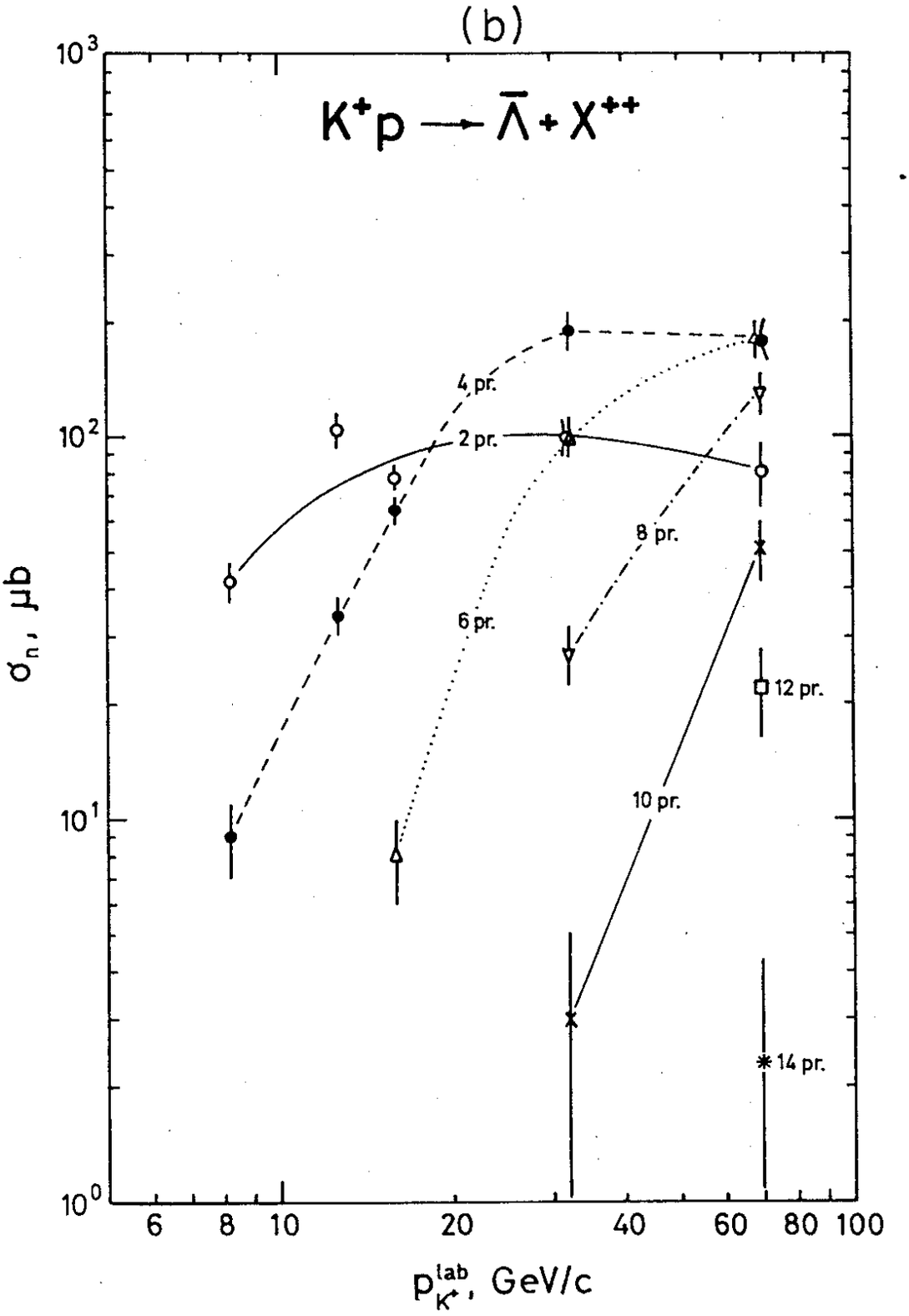
(b)
$K^+p \rightarrow \bar{\Lambda} + X^{++}$
10^3
10^2
10^1
10^0
σ_n, μb
4 pr.
2 pr.
6 pr.
8 pr.
12 pr.
10 pr.
14 pr.
6
8
10
20
40
60
80
100
$p_{K^+}^{lab}$, GeV/c

Fig. 2(b)

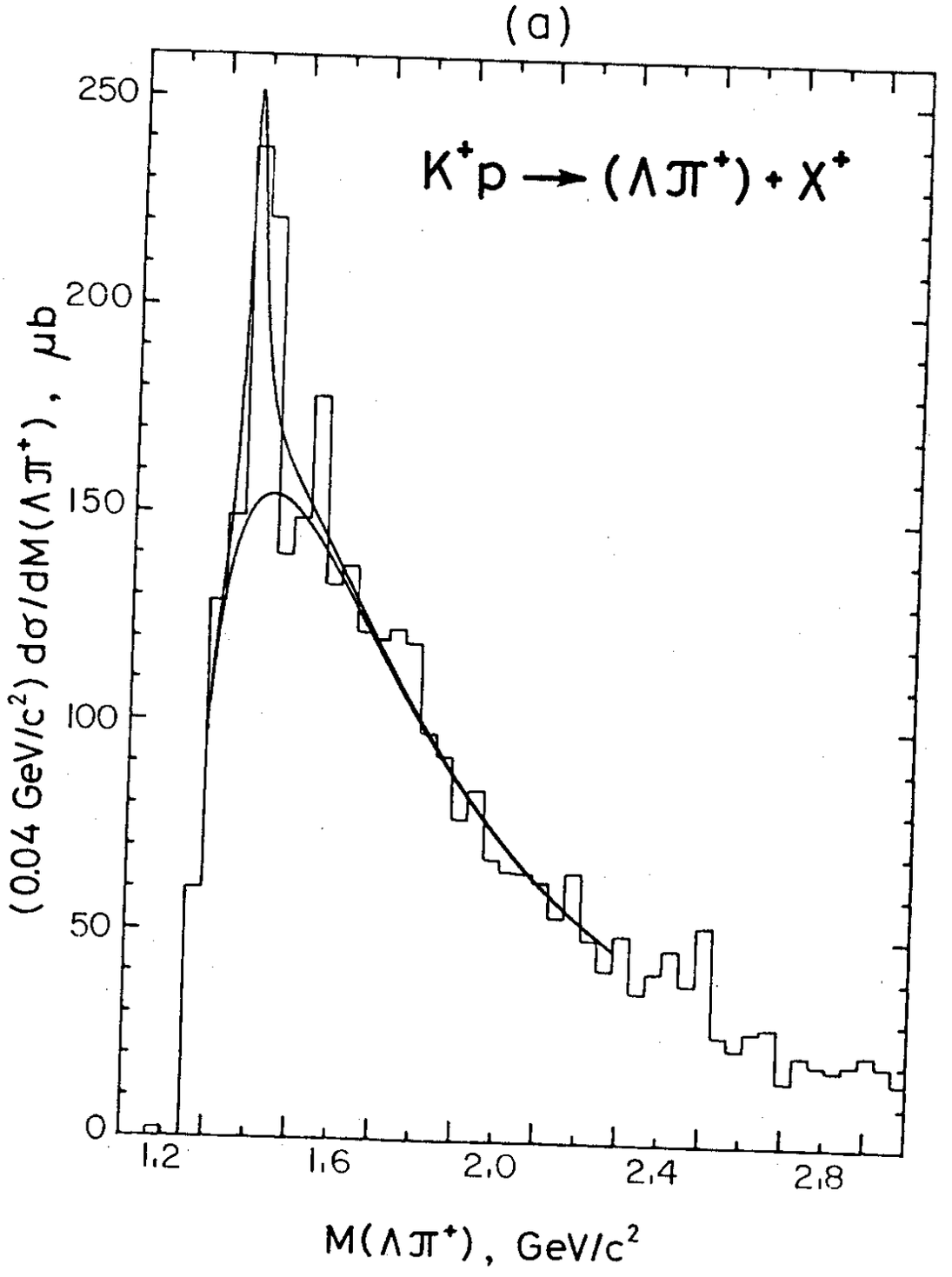
(a)
$K^+p \rightarrow (\Lambda\pi^+) + X^+$
250
200
150
100
50
0
$(0.04\ GeV/c^2)\ d\sigma/dM(\Lambda\pi^+),\ \mu b$
1.2
1.6
2.0
2.4
2.8
$M(\Lambda\pi^+),\ GeV/c^2$

Fig. 3(a)

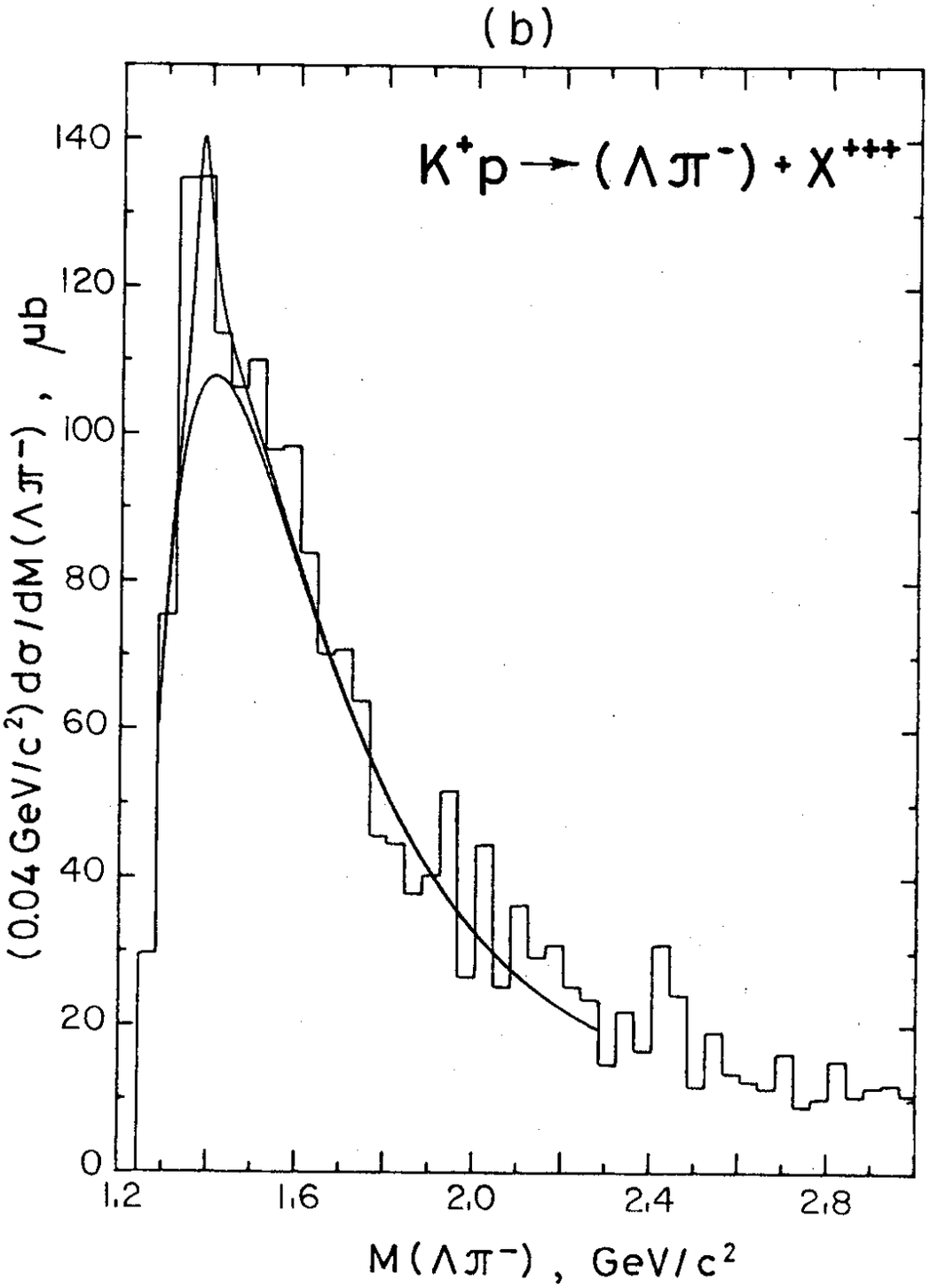
(b)
$K^+p \rightarrow (\Lambda\pi^-) + X^{+++}$
$(0.04\,GeV/c^2)\,d\sigma/dM(\Lambda\pi^-)$, μb
$M(\Lambda\pi^-)$, GeV/c^2
0
20
40
60
80
100
120
140
1.2
1.6
2.0
2.4
2.8

Fig. 3(b)

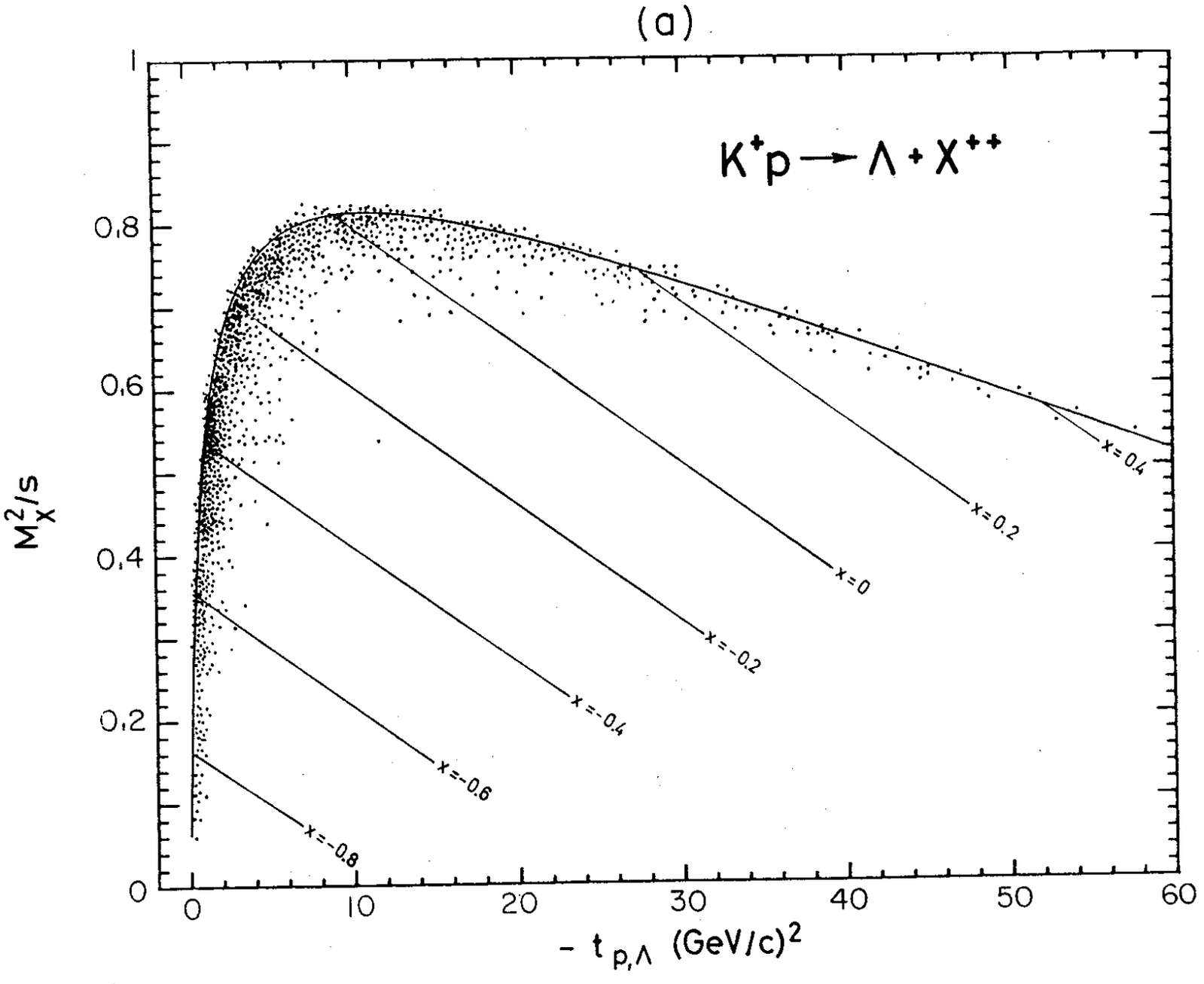
(a)
$K^+p \rightarrow \Lambda + X^{++}$
M_X^2/s
$-t_{p,\Lambda}$ (GeV/c)^2
x=0.4
x=0.2
x=0
x=-0.2
x=-0.4
x=-0.6
x=-0.8
0
0.2
0.4
0.6
0.8
1
0
10
20
30
40
50
60

Fig. 4(a)

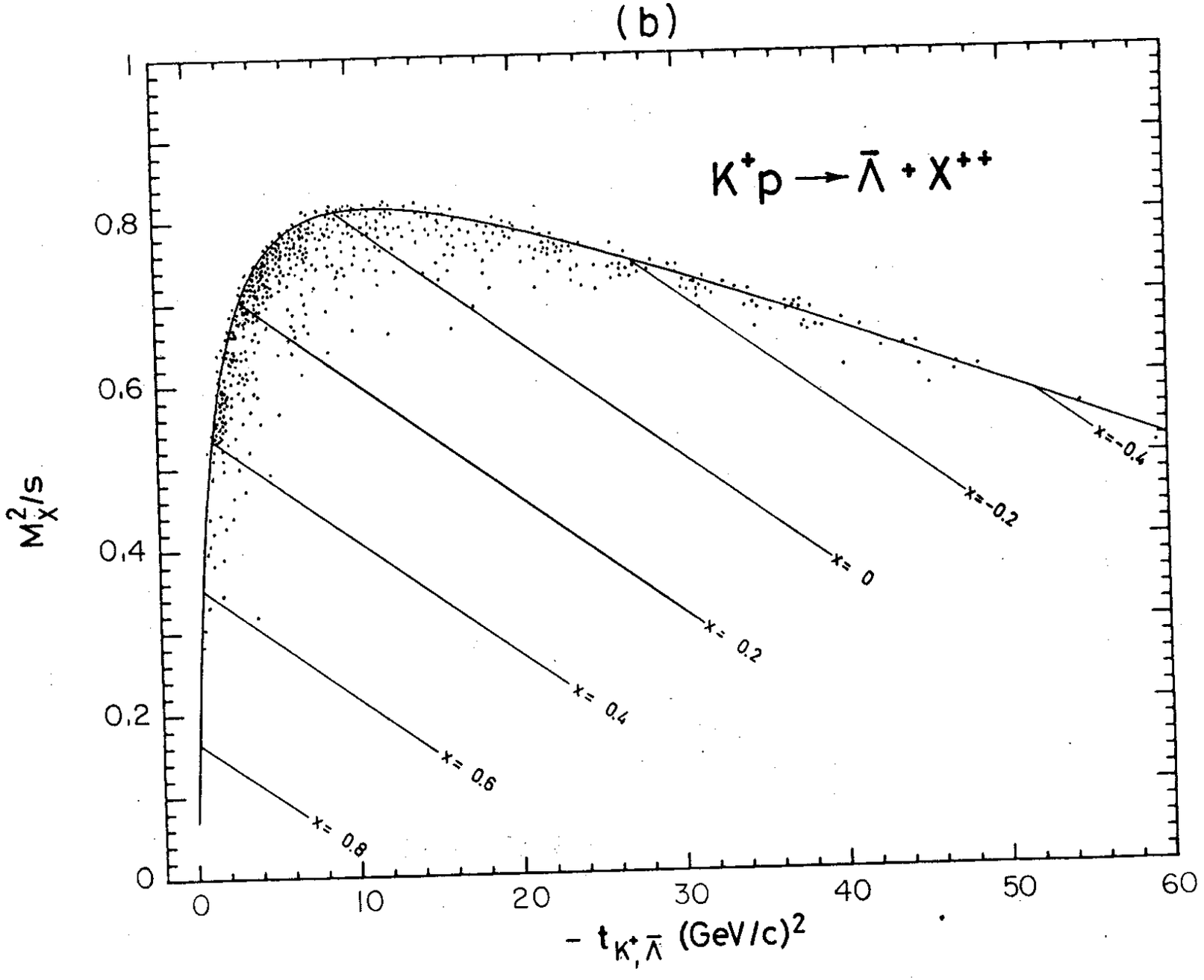
(b)
$K^+p \rightarrow \bar{\Lambda} + X^{++}$
M_X^2/s
$-t_{K^+,\bar{\Lambda}}$ (GeV/c)^2
x=-0.4
x=-0.2
x= 0
x= 0.2
x= 0.4
x= 0.6
x= 0.8
0
0.2
0.4
0.6
0.8
1
0
10
20
30
40
50
60

Fig. 4(b)

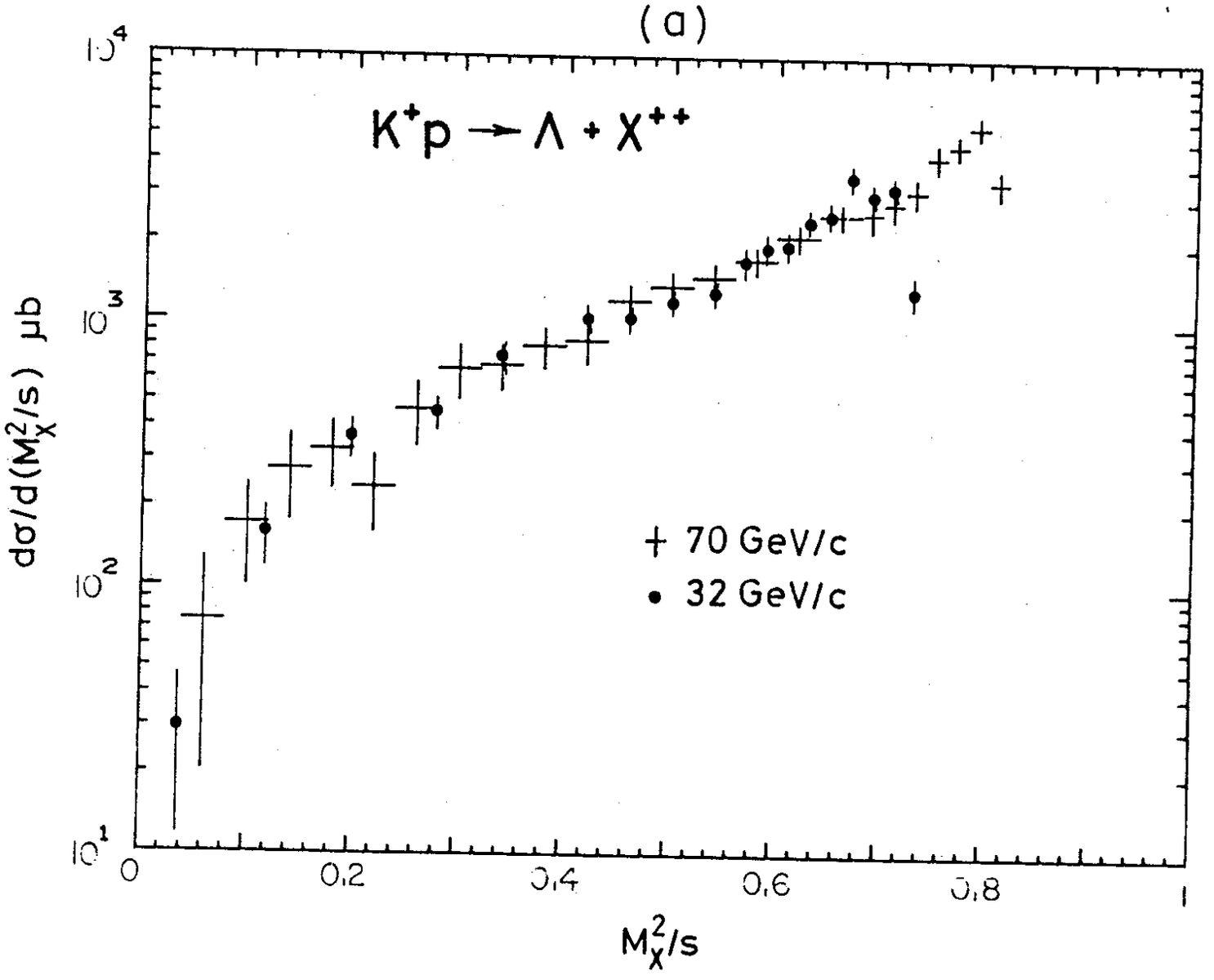
(a)
$K^+p \rightarrow \Lambda + X^{++}$
+ 70 GeV/c
• 32 GeV/c
$d\sigma/d(M_X^2/s)$ μb
M_X^2/s
10^4
10^3
10^2
10^1
0
0.2
0.4
0.6
0.8
1

Fig. 5(a)

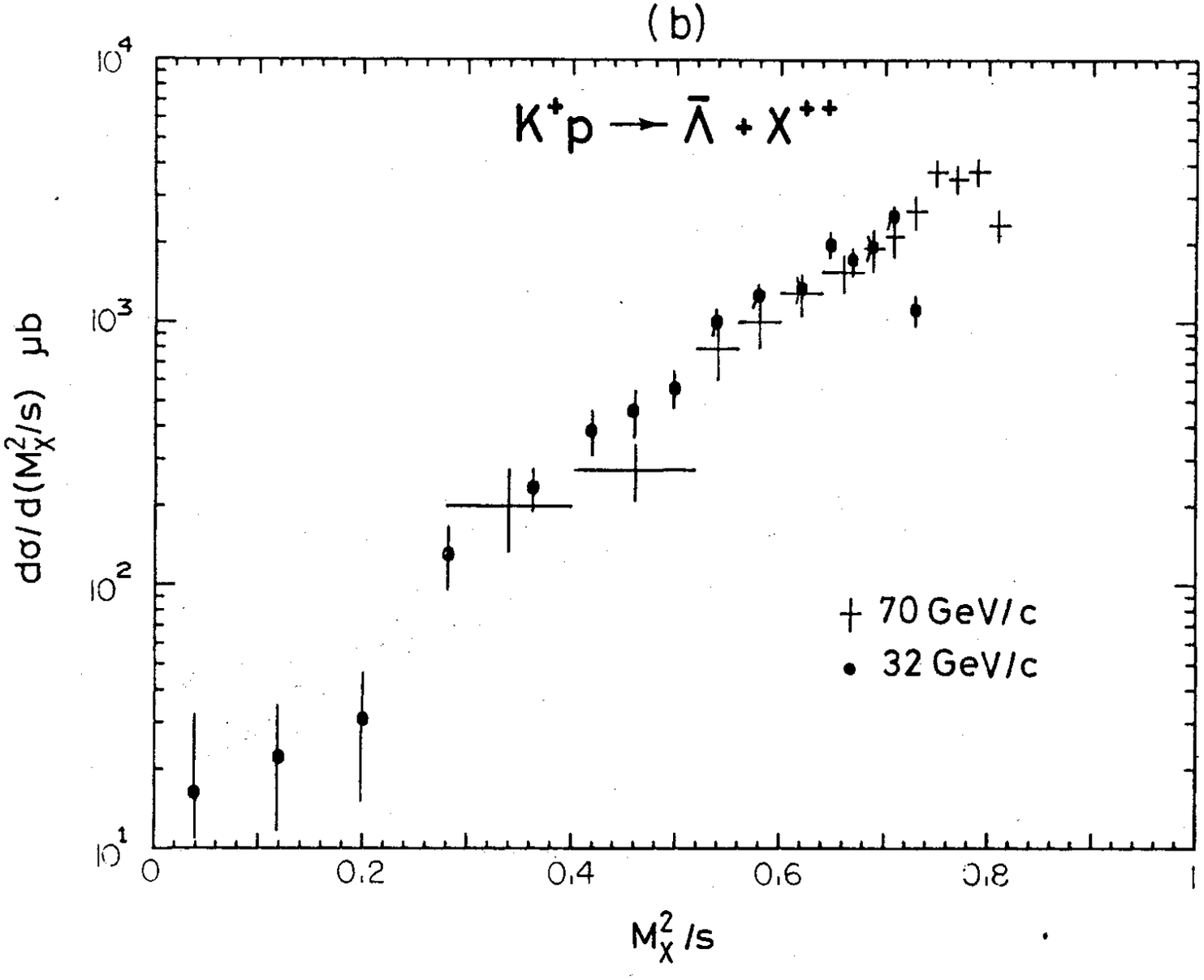
(b)
$K^+p \rightarrow \bar{\Lambda} + X^{++}$
$d\sigma/d(M_X^2/s)$ μb
10^4
10^3
10^2
10^1
0
0.2
0.4
0.6
0.8
1
M_X^2/s
+ 70 GeV/c
• 32 GeV/c

Fig. 5(b)

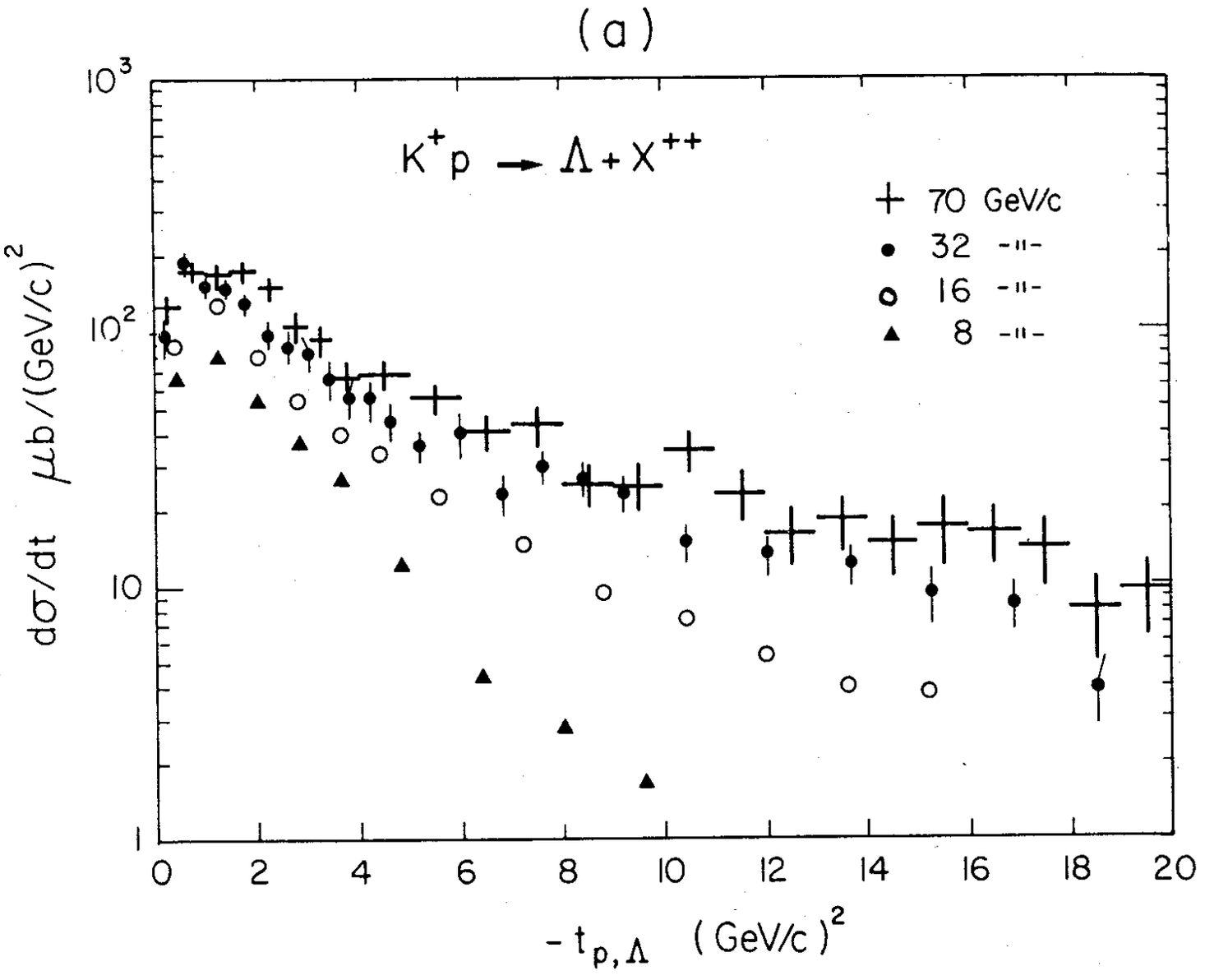
(a)
$K^+p \rightarrow \Lambda + X^{++}$
70 GeV/c
32 -"-
16 -"-
8 -"-
$d\sigma/dt$ $\mu b/(GeV/c)^2$
10^3
10^2
10
1
0
2
4
6
8
10
12
14
16
18
20
$-t_{p,\Lambda}$ $(GeV/c)^2$

Fig. 6(a)

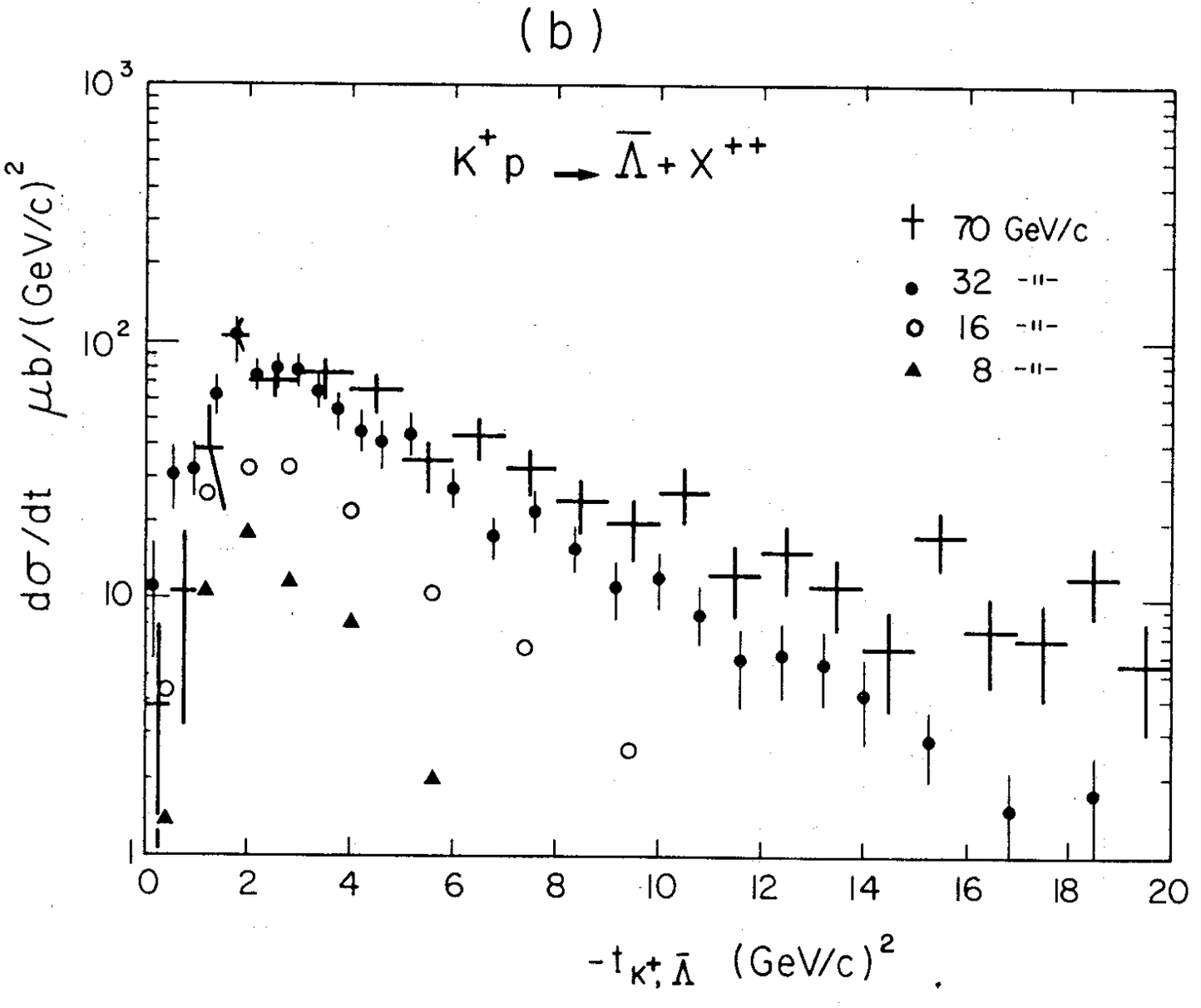
(b)
$K^+ p \rightarrow \bar{\Lambda} + X^{++}$
70 GeV/c
32 -"-
16 -"-
8 -"-
$d\sigma/dt \quad \mu b/(GeV/c)^2$
10^3
10^2
10
1
0
2
4
6
8
10
12
14
16
18
20
$-t_{K^+,\bar{\Lambda}} \quad (GeV/c)^2$

Fig. 6(b)

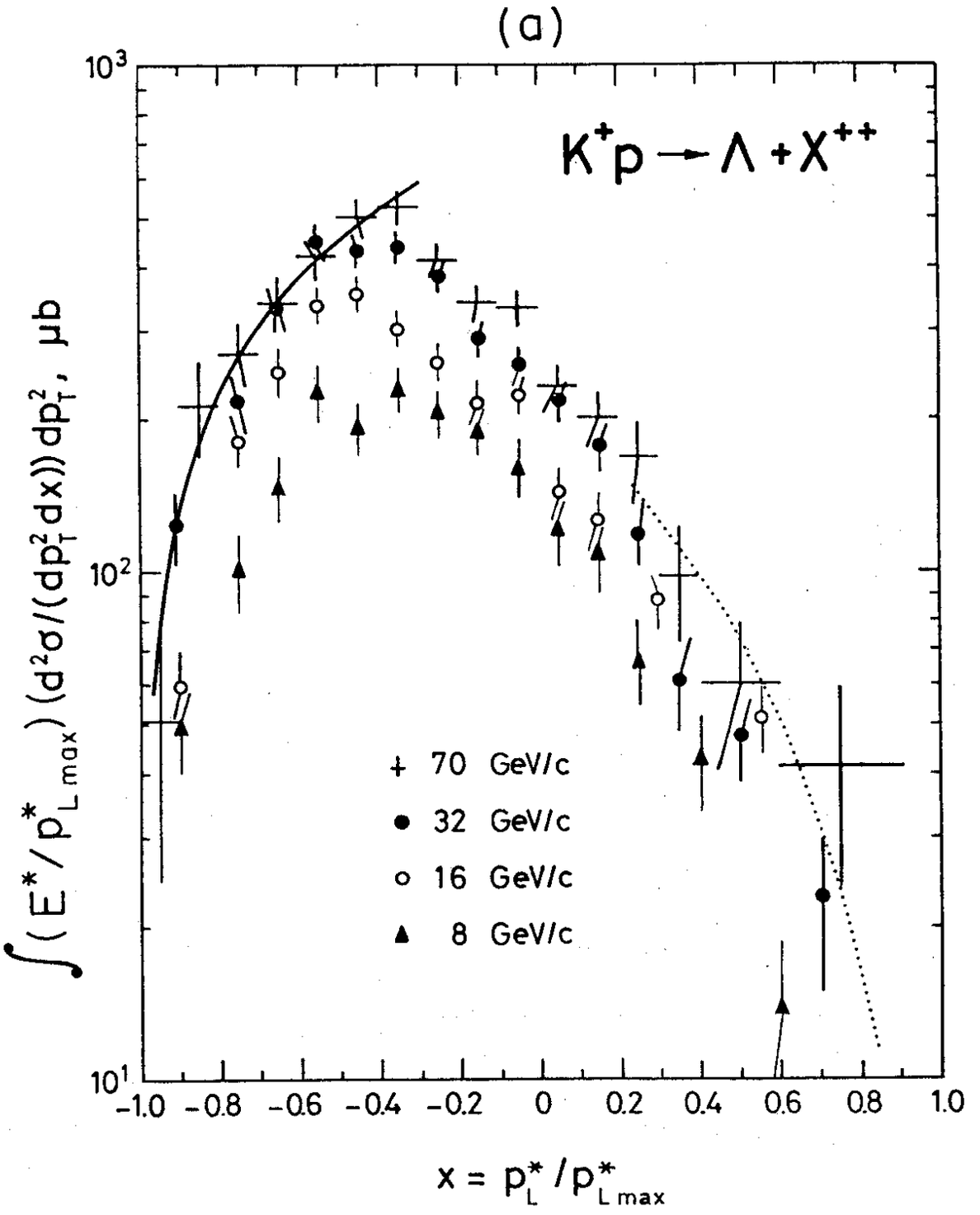
(a)
$K^+p \rightarrow \Lambda + X^{++}$
$\int (E^*/p^*_{L\,max})(d^2\sigma/(dp_T^2\,dx))\,dp_T^2$, μb
10^3
10^2
10^1
-1.0 -0.8 -0.6 -0.4 -0.2 0 0.2 0.4 0.6 0.8 1.0
$x = p^*_L / p^*_{L\,max}$
+ 70 GeV/c
● 32 GeV/c
○ 16 GeV/c
▲ 8 GeV/c

Fig. 7(a)

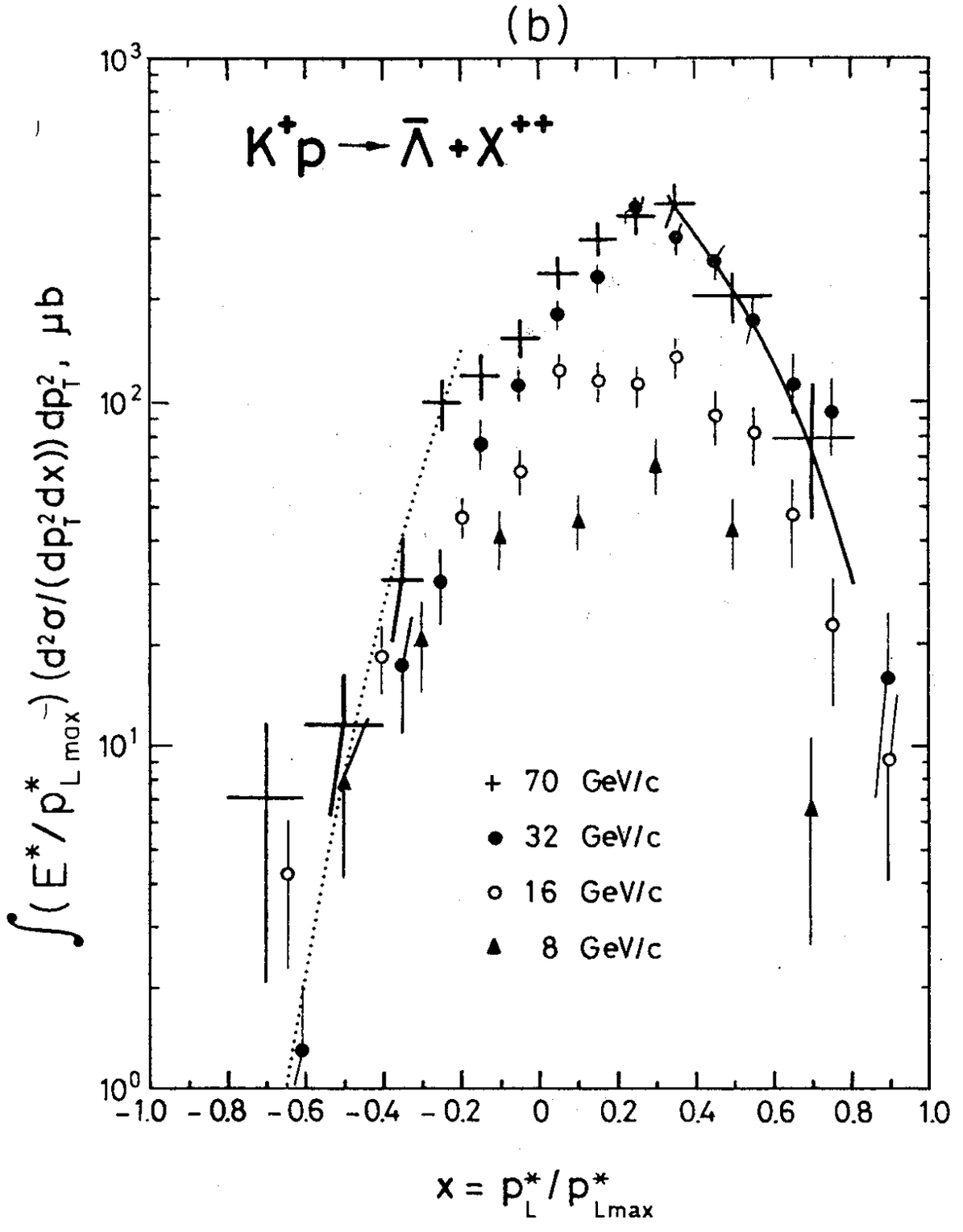
(b)
$K^+p \rightarrow \bar{\Lambda} + X^{++}$
$\int (E^*/p^*_{L\,max})^{-1} (d^2\sigma/(dp_T^2 dx))\, dp_T^2$, μb
10^3
10^2
10^1
10^0
+ 70 GeV/c
● 32 GeV/c
○ 16 GeV/c
▲ 8 GeV/c
-1.0 -0.8 -0.6 -0.4 -0.2 0 0.2 0.4 0.6 0.8 1.0
$x = p^*_L / p^*_{Lmax}$

Fig. 7(b)

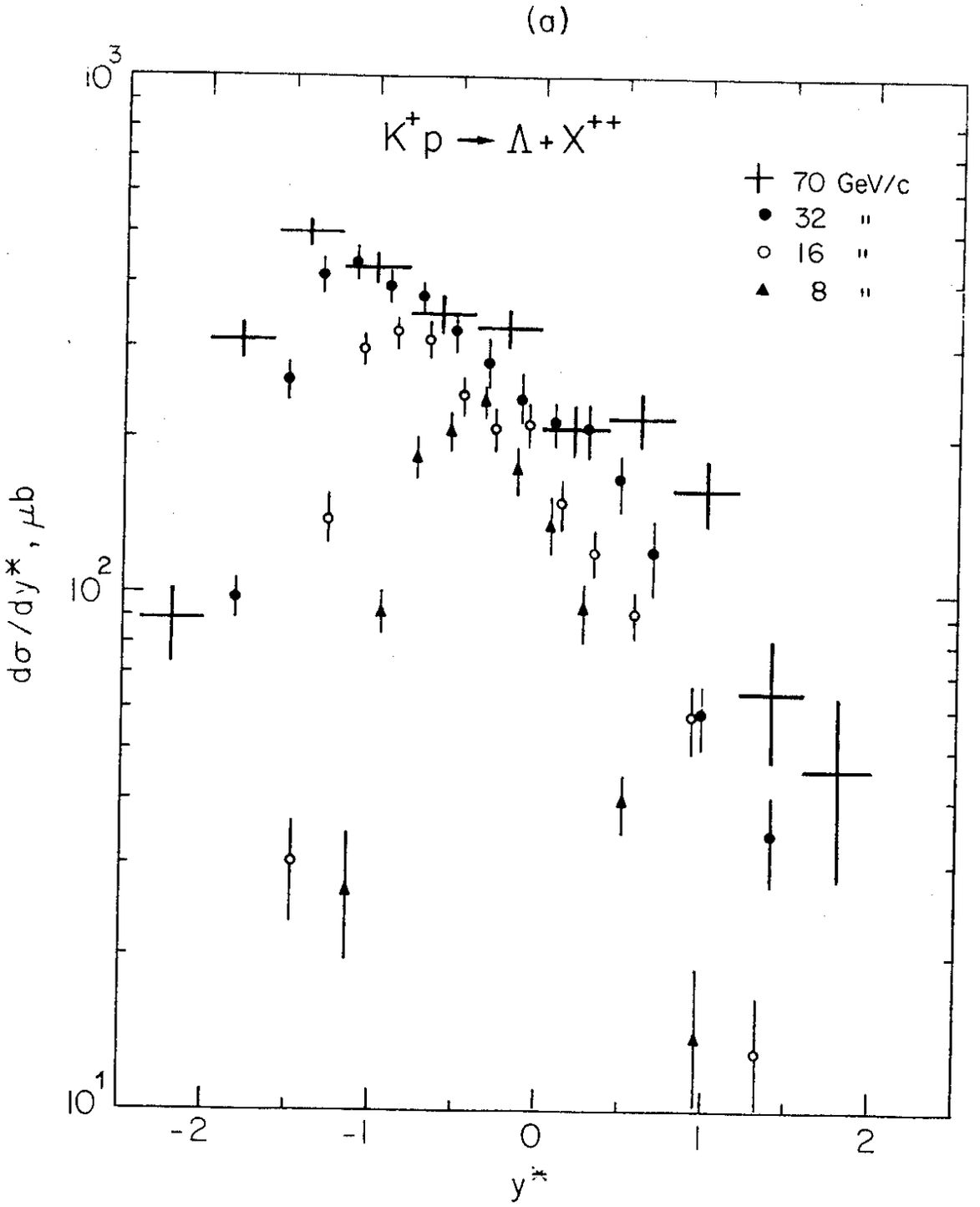
(a)
$K^+p \rightarrow \Lambda + X^{++}$
70 GeV/c
32 "
16 "
8 "
$d\sigma/dy^*$, μb
y^*
10^3
10^2
10^1
-2
-1
0
1
2

Fig. 8(a)

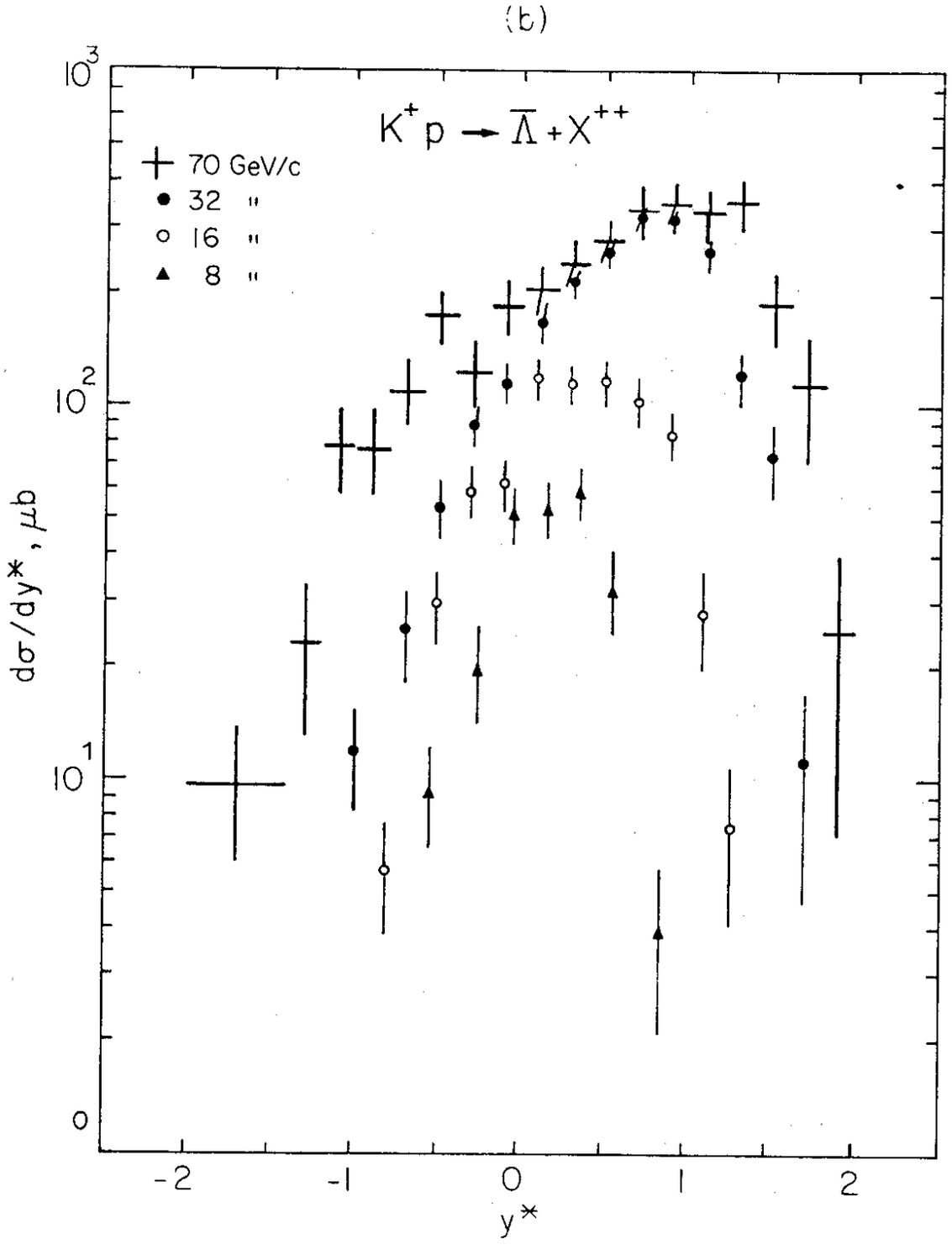
(b)
$K^+p \rightarrow \bar{\Lambda} + X^{++}$
70 GeV/c
32 "
16 "
8 "
$d\sigma/dy^*$, μb
10^3
10^2
10^1
0
-2
-1
0
1
2
y^*

Fig. 8(b)

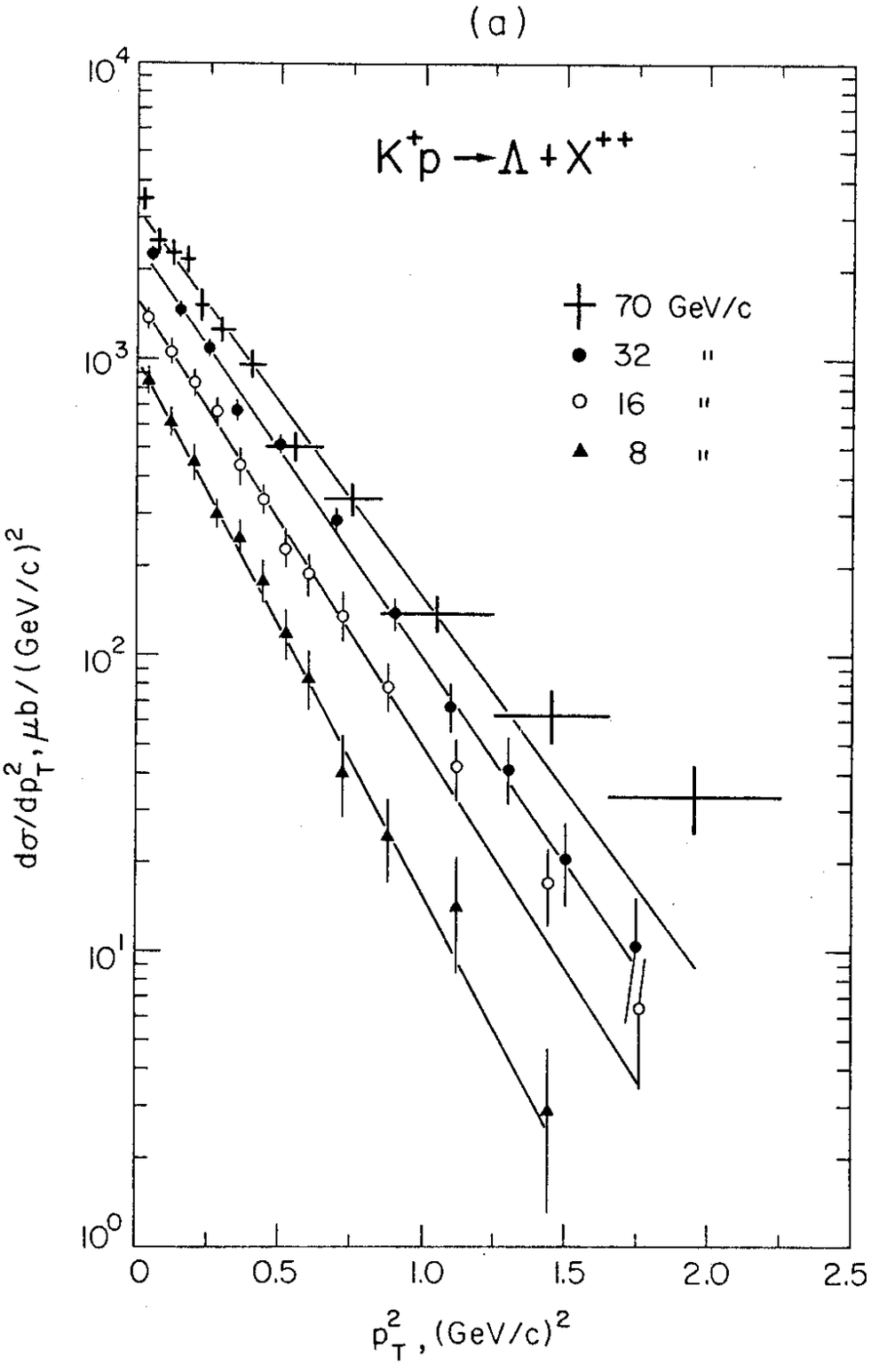
(a)
$K^+p \rightarrow \Lambda + X^{++}$
70 GeV/c
32 "
16 "
8 "
$d\sigma/dp_T^2, \mu b/(GeV/c)^2$
$p_T^2, (GeV/c)^2$
10^4
10^3
10^2
10^1
10^0
0
0.5
1.0
1.5
2.0
2.5

Fig. 9(a)

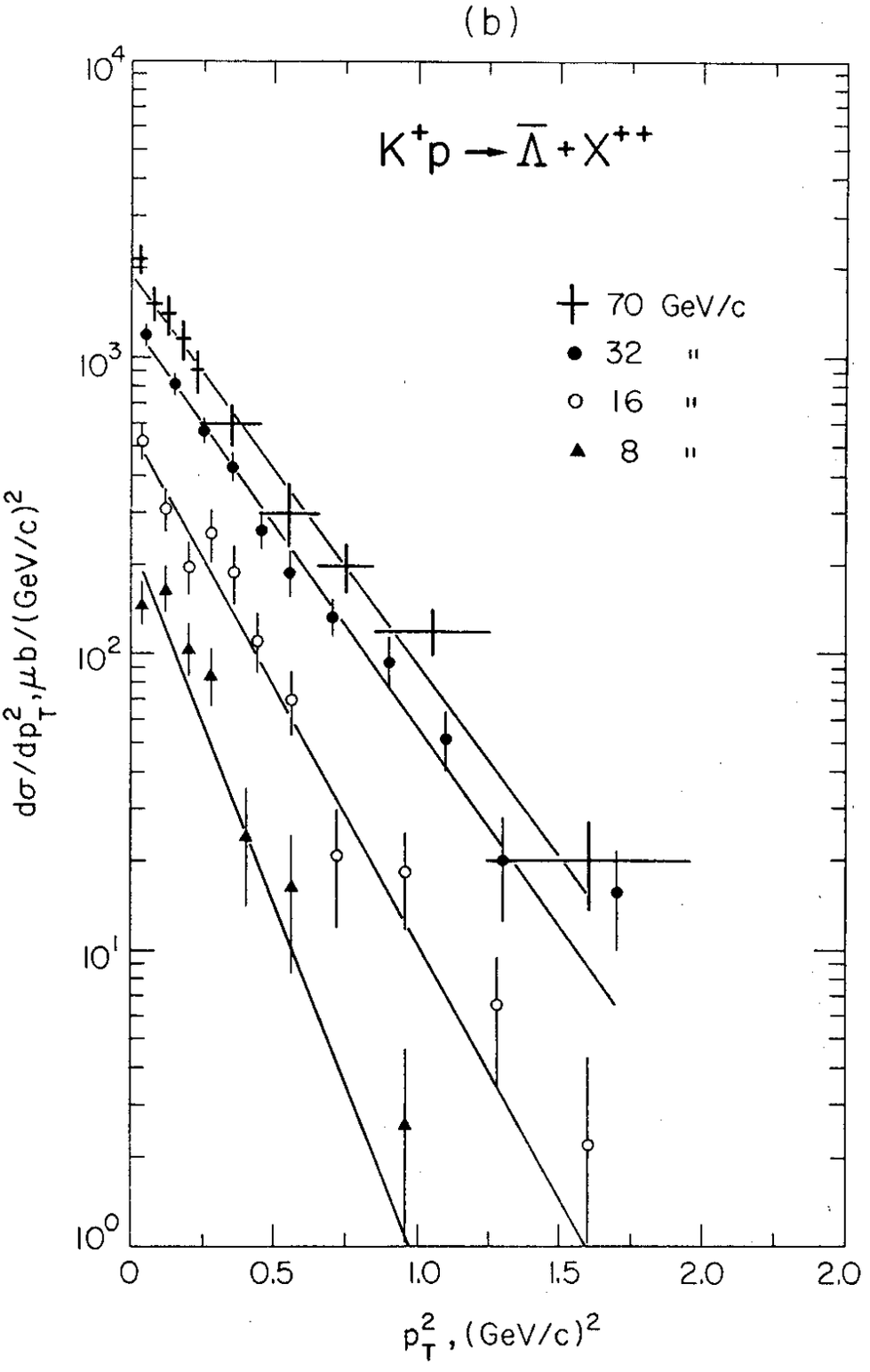
(b)
$K^+p \rightarrow \bar{\Lambda} + X^{++}$
70 GeV/c
32 "
16 "
8 "
$d\sigma/dp_T^2, \mu b/(GeV/c)^2$
$p_T^2, (GeV/c)^2$
10^4
10^3
10^2
10^1
10^0
0
0.5
1.0
1.5
2.0
2.0

Fig. 9(b)

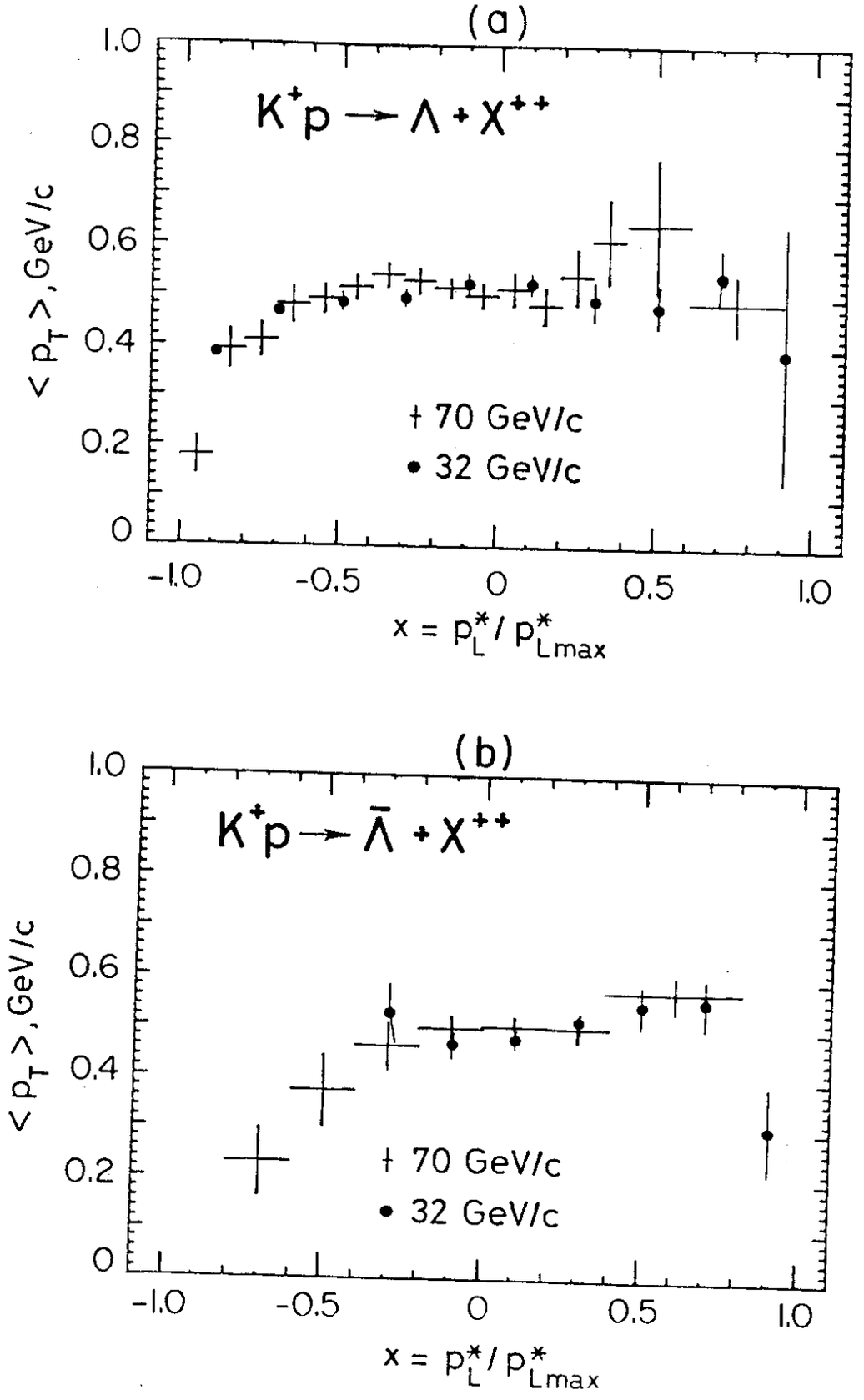
(a)
$K^+p \rightarrow \Lambda + X^{++}$
$< p_T >$, GeV/c
+ 70 GeV/c
• 32 GeV/c
$x = p_L^* / p_{Lmax}^*$
(b)
$K^+p \rightarrow \bar{\Lambda} + X^{++}$
$< p_T >$, GeV/c
+ 70 GeV/c
• 32 GeV/c
$x = p_L^* / p_{Lmax}^*$

Fig. 10

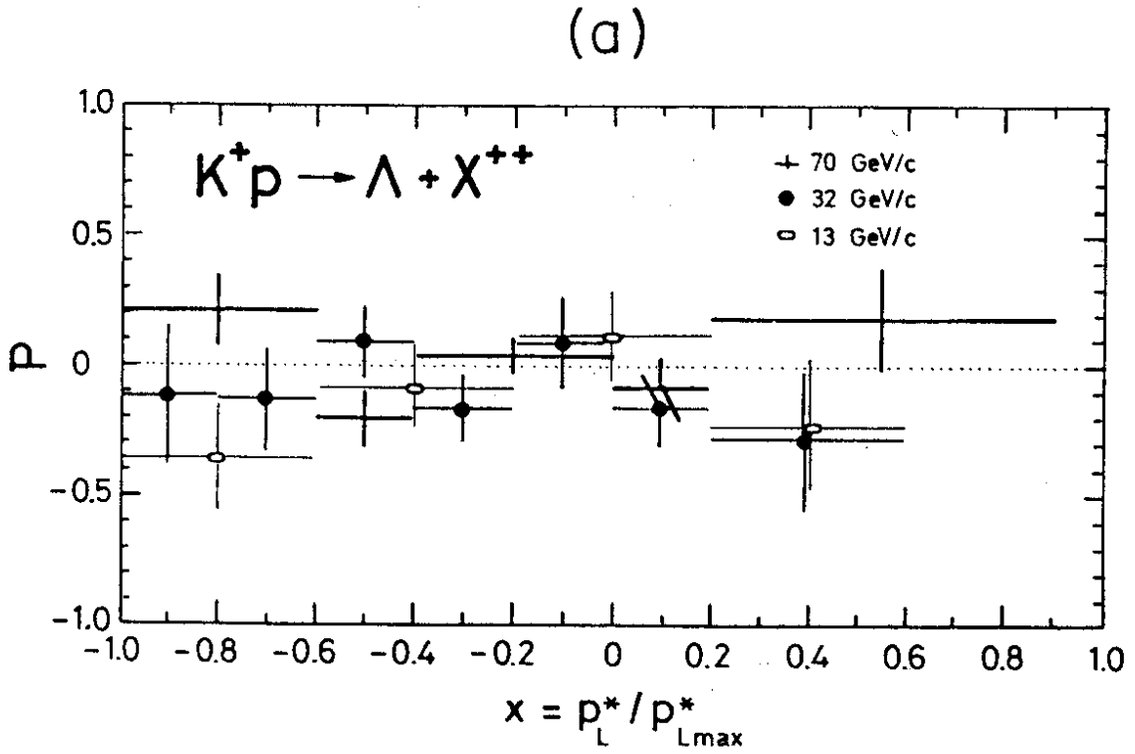
(a)
$K^+p \rightarrow \Lambda + X^{++}$
70 GeV/c
32 GeV/c
13 GeV/c
P
1.0
0.5
0
-0.5
-1.0
-1.0 -0.8 -0.6 -0.4 -0.2 0 0.2 0.4 0.6 0.8 1.0
$x = p^*_L / p^*_{Lmax}$

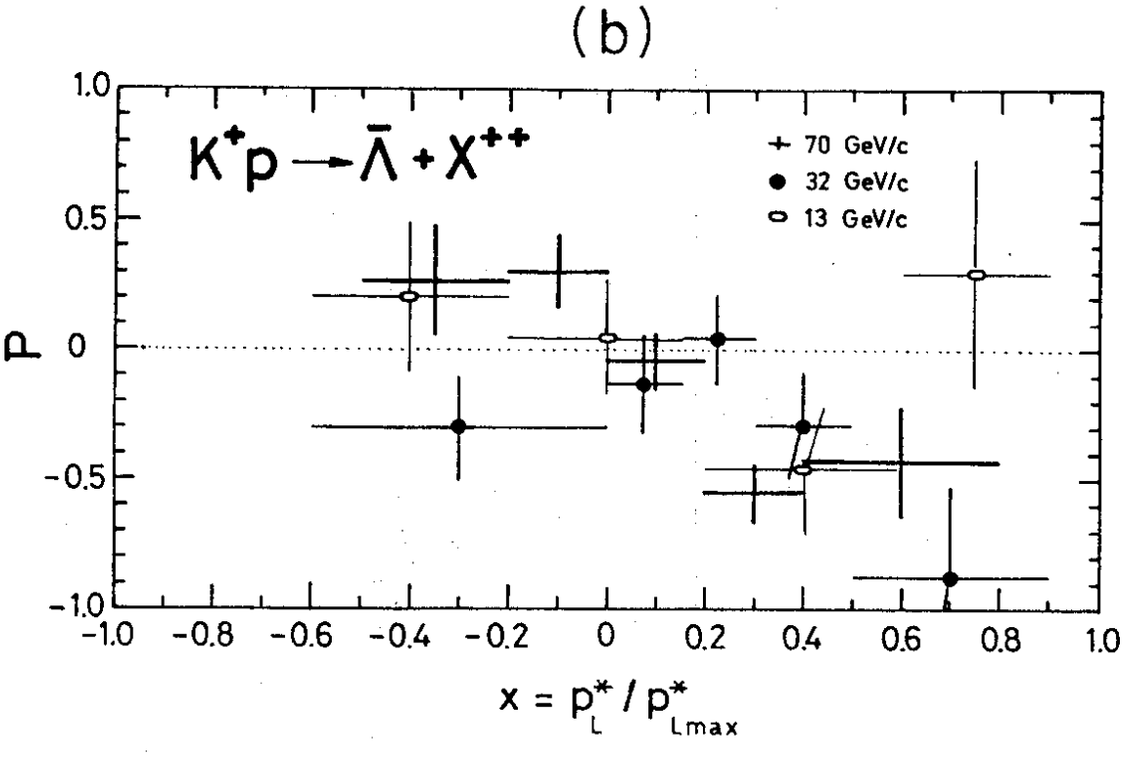
(b)
$K^+p \rightarrow \bar{\Lambda} + X^{++}$
70 GeV/c
32 GeV/c
13 GeV/c
P
1.0
0.5
0
-0.5
-1.0
-1.0 -0.8 -0.6 -0.4 -0.2 0 0.2 0.4 0.6 0.8 1.0
$x = p^*_L / p^*_{Lmax}$

Fig. 11

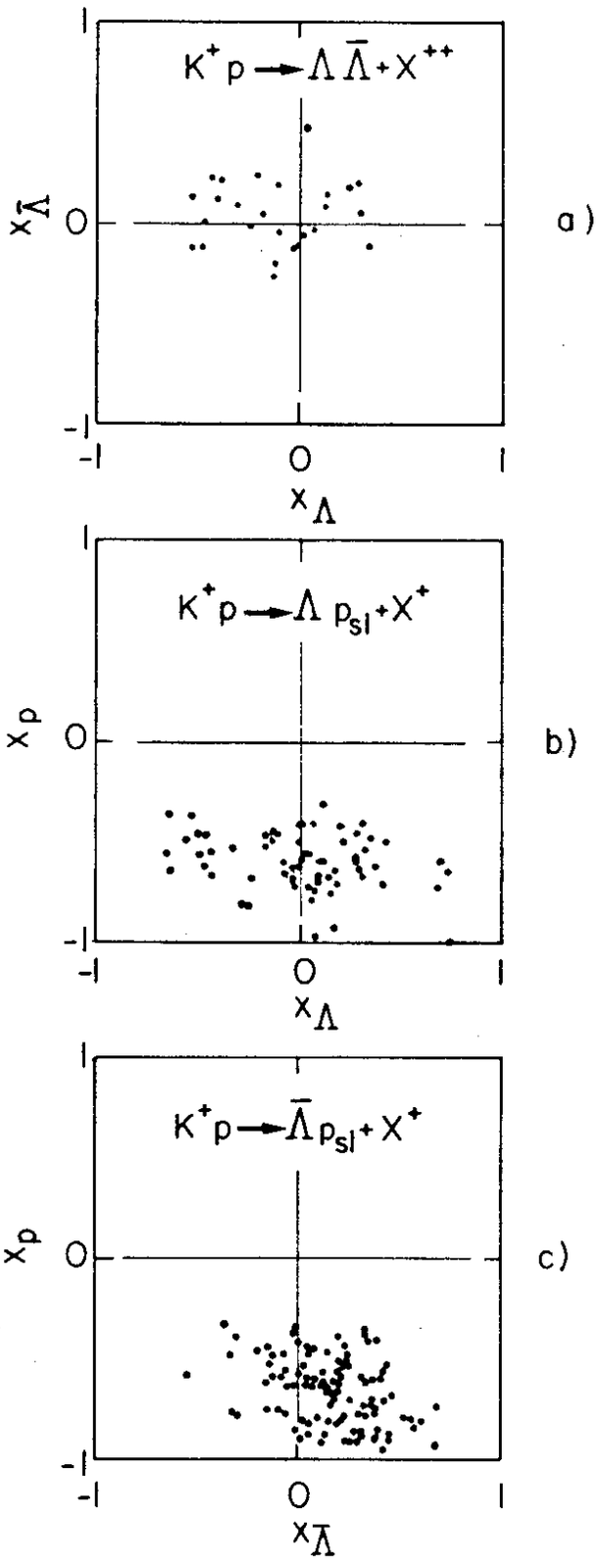
$K^+p \rightarrow \Lambda\bar{\Lambda}+X^{++}$
$x_{\bar{\Lambda}}$
x_Λ
a)
$K^+p \rightarrow \Lambda\, p_{sl}+X^+$
x_p
x_Λ
b)
$K^+p \rightarrow \bar{\Lambda}\, p_{sl}+X^+$
x_p
$x_{\bar{\Lambda}}$
c)
0
-1
1

Fig. 12